View metadata, citation and similar papers at core.ac.uk
brought to you by CORE
provided by CERN Document Server

DESY-02-113

Measurement of high-Q^2 e^-p neutral current cross sections at HERA and the extraction of xF_3

ZEUS Collaboration

Abstract

Cross sections for e^-p neutral current deep inelastic scattering have been measured at a centre-of-mass energy of 318 GeV using an integrated luminosity of 15.9 pb^{-1} collected with the ZEUS detector at HERA. Results on the double-differential cross-section $d^2\sigma/dx\,dQ^2$ in the range $185 < Q^2 < 50\,000\,\mathrm{GeV}^2$ and $0.0037 < x < 0.75$, as well as the single-differential cross-sections $d\sigma/dQ^2$, $d\sigma/dx$ and $d\sigma/dy$ for $Q^2 > 200\,\mathrm{GeV}^2$, are presented. To study the effect of Z-boson exchange, $d\sigma/dx$ has also been measured for $Q^2 > 10\,000\,\mathrm{GeV}^2$. The structure function xF_3 has been extracted by combining the e^-p results presented here with the recent ZEUS measurements of e^+p neutral current deep inelastic scattering. All results agree well with the predictions of the Standard Model.

The ZEUS Collaboration

S. Chekanov, D. Krakauer, S. Magill, B. Musgrave, J. Repond, R. Yoshida
Argonne National Laboratory, Argonne, Illinois 60439-4815 [n]

M.C.K. Mattingly
Andrews University, Berrien Springs, Michigan 49104-0380

P. Antonioli, G. Bari, M. Basile, L. Bellagamba, D. Boscherini, A. Bruni, G. Bruni, G. Cara Romeo, L. Cifarelli, F. Cindolo, A. Contin, M. Corradi, S. De Pasquale, P. Giusti, G. Iacobucci, A. Margotti, R. Nania, F. Palmonari, A. Pesci, G. Sartorelli, A. Zichichi
University and INFN Bologna, Bologna, Italy [e]

G. Aghuzumtsyan, D. Bartsch, I. Brock, J. Crittenden[1], S. Goers, H. Hartmann, E. Hilger, P. Irrgang, H.-P. Jakob, A. Kappes, U.F. Katz[2], R. Kerger[3], O. Kind, E. Paul, J. Rautenberg[4], R. Renner, H. Schnurbusch, A. Stifutkin, J. Tandler, K.C. Voss, A. Weber
Physikalisches Institut der Universität Bonn, Bonn, Germany [b]

D.S. Bailey[5], N.H. Brook[5], J.E. Cole, B. Foster, G.P. Heath, H.F. Heath, S. Robins, E. Rodrigues[6], J. Scott, R.J. Tapper, M. Wing
H.H. Wills Physics Laboratory, University of Bristol, Bristol, United Kingdom [m]

M. Capua, A. Mastroberardino, M. Schioppa, G. Susinno
Calabria University, Physics Department and INFN, Cosenza, Italy [e]

J.Y. Kim, Y.K. Kim, J.H. Lee, I.T. Lim, M.Y. Pac[7]
Chonnam National University, Kwangju, Korea [g]

A. Caldwell[8], M. Helbich, X. Liu, B. Mellado, Y. Ning, S. Paganis, Z. Ren, W.B. Schmidke, F. Sciulli
Nevis Laboratories, Columbia University, Irvington on Hudson, New York 10027 [o]

J. Chwastowski, A. Eskreys, J. Figiel, K. Olkiewicz, K. Piotrzkowski[9], M.B. Przybycień[10], P. Stopa, L. Zawiejski
Institute of Nuclear Physics, Cracow, Poland [i]

L. Adamczyk, T. Bołd, I. Grabowska-Bołd, D. Kisielewska, A.M. Kowal, M. Kowal, T. Kowalski, M. Przybycień, L. Suszycki, D. Szuba, J. Szuba[11]
Faculty of Physics and Nuclear Techniques, University of Mining and Metallurgy, Cracow, Poland [p]

A. Kotański[12], W. Słomiński[13]
Department of Physics, Jagellonian University, Cracow, Poland

L.A.T. Bauerdick[14], U. Behrens, K. Borras, D.G. Cassel[15], V. Chiochia, D. Dannheim, M. Derrick[16], G. Drews, J. Fourletova, A. Fox-Murphy, U. Fricke, A. Geiser, F. Goebel[8], P. Göttlicher[17], O. Gutsche, T. Haas, W. Hain, G.F. Hartner, S. Hillert, U. Kötz, H. Kowalski[18], G. Kramberger, H. Labes, D. Lelas, B. Löhr, R. Mankel, M. Martínez[14], I.-A. Melzer-Pellmann, M. Moritz, D. Notz, M.C. Petrucci[19], A. Polini, A. Raval, U. Schneekloth, F. Selonke[20], B. Surrow[21], H. Wessoleck, R. Wichmann[22], G. Wolf, C. Youngman, W. Zeuner
Deutsches Elektronen-Synchrotron DESY, Hamburg, Germany

A. Lopez-Duran Viani[23], A. Meyer, S. Schlenstedt
DESY Zeuthen, Zeuthen, Germany

G. Barbagli, E. Gallo, C. Genta, P. G. Pelfer
University and INFN, Florence, Italy [e]

A. Bamberger, A. Benen, N. Coppola, H. Raach
Fakultät für Physik der Universität Freiburg i.Br., Freiburg i.Br., Germany [b]

M. Bell, P.J. Bussey, A.T. Doyle, C. Glasman, S. Hanlon, S.W. Lee, A. Lupi, G.J. McCance, D.H. Saxon, I.O. Skillicorn
Department of Physics and Astronomy, University of Glasgow, Glasgow, United Kingdom [m]

I. Gialas
Department of Engineering in Management and Finance, Univ. of Aegean, Greece

B. Bodmann, T. Carli, U. Holm, K. Klimek, N. Krumnack, E. Lohrmann, M. Milite, H. Salehi, S. Stonjek[24], K. Wick, A. Ziegler, Ar. Ziegler
Hamburg University, Institute of Exp. Physics, Hamburg, Germany [b]

C. Collins-Tooth, C. Foudas, R. Gonçalo[6], K.R. Long, F. Metlica, D.B. Miller, A.D. Tapper, R. Walker
Imperial College London, High Energy Nuclear Physics Group, London, United Kingdom [m]

P. Cloth, D. Filges
Forschungszentrum Jülich, Institut für Kernphysik, Jülich, Germany

M. Kuze, K. Nagano, K. Tokushuku[25], S. Yamada, Y. Yamazaki
Institute of Particle and Nuclear Studies, KEK, Tsukuba, Japan [f]

A.N. Barakbaev, E.G. Boos, N.S. Pokrovskiy, B.O. Zhautykov
Institute of Physics and Technology of Ministry of Education and Science of Kazakhstan, Almaty, Kazakhstan

H. Lim, D. Son
Kyungpook National University, Taegu, Korea [g]

F. Barreiro, O. González, L. Labarga, J. del Peso, I. Redondo[26], J. Terrón, M. Vázquez
Departamento de Física Teórica, Universidad Autónoma Madrid,Madrid, Spain [l]

M. Barbi, A. Bertolin, F. Corriveau, A. Ochs, S. Padhi, D.G. Stairs, M. St-Laurent
Department of Physics, McGill University, Montréal, Québec, Canada H3A 2T8 [a]

T. Tsurugai
Meiji Gakuin University, Faculty of General Education, Yokohama, Japan

A. Antonov, P. Danilov, B.A. Dolgoshein, D. Gladkov, V. Sosnovtsev, S. Suchkov
Moscow Engineering Physics Institute, Moscow, Russia [j]

R.K. Dementiev, P.F. Ermolov, Yu.A. Golubkov, I.I. Katkov, L.A. Khein, I.A. Korzhavina, V.A. Kuzmin, B.B. Levchenko, O.Yu. Lukina, A.S. Proskuryakov, L.M. Shcheglova, N.N. Vlasov, S.A. Zotkin
Moscow State University, Institute of Nuclear Physics, Moscow, Russia [k]

C. Bokel, J. Engelen, S. Grijpink, E. Koffeman, P. Kooijman, E. Maddox, A. Pellegrino, S. Schagen, E. Tassi, H. Tiecke, N. Tuning, J.J. Velthuis, L. Wiggers, E. de Wolf
NIKHEF and University of Amsterdam, Amsterdam, Netherlands [h]

N. Brümmer, B. Bylsma, L.S. Durkin, J. Gilmore, C.M. Ginsburg, C.L. Kim, T.Y. Ling
Physics Department, Ohio State University, Columbus, Ohio 43210 [n]

S. Boogert, A.M. Cooper-Sarkar, R.C.E. Devenish, J. Ferrando, G. Grzelak, T. Matsushita, M. Rigby, O. Ruske[27], M.R. Sutton, R. Walczak
Department of Physics, University of Oxford, Oxford United Kingdom [m]

R. Brugnera, R. Carlin, F. Dal Corso, S. Dusini, A. Garfagnini, S. Limentani, A. Longhin, A. Parenti, M. Posocco, L. Stanco, M. Turcato
Dipartimento di Fisica dell' Università and INFN, Padova, Italy [e]

E.A. Heaphy, B.Y. Oh, P.R.B. Saull[28], J.J. Whitmore[29]
Department of Physics, Pennsylvania State University, University Park, Pennsylvania 16802 [o]

Y. Iga
Polytechnic University, Sagamihara, Japan [f]

G. D'Agostini, G. Marini, A. Nigro
Dipartimento di Fisica, Università 'La Sapienza' and INFN, Rome, Italy [e]

C. Cormack[30], J.C. Hart, N.A. McCubbin
Rutherford Appleton Laboratory, Chilton, Didcot, Oxon, United Kingdom [m]

C. Heusch
University of California, Santa Cruz, California 95064 [n]

I.H. Park
Department of Physics, Ewha Womans University, Seoul, Korea

N. Pavel
Fachbereich Physik der Universität-Gesamthochschule Siegen, Germany

H. Abramowicz, A. Gabareen, S. Kananov, A. Kreisel, A. Levy
Raymond and Beverly Sackler Faculty of Exact Sciences, School of Physics, Tel-Aviv University, Tel-Aviv, Israel [d]

T. Abe, T. Fusayasu, S. Kagawa, T. Kohno, T. Tawara, T. Yamashita
Department of Physics, University of Tokyo, Tokyo, Japan [f]

R. Hamatsu, T. Hirose[20], M. Inuzuka, S. Kitamura[31], K. Matsuzawa, T. Nishimura
Tokyo Metropolitan University, Deptartment of Physics, Tokyo, Japan [f]

M. Arneodo[32], N. Cartiglia, R. Cirio, M. Costa, M.I. Ferrero, S. Maselli, V. Monaco, C. Peroni, M. Ruspa, R. Sacchi, A. Solano, A. Staiano
Università di Torino, Dipartimento di Fisica Sperimentale and INFN, Torino, Italy [e]

R. Galea, T. Koop, G.M. Levman, J.F. Martin, A. Mirea, A. Sabetfakhri
Department of Physics, University of Toronto, Toronto, Ontario, Canada M5S 1A7 [a]

J.M. Butterworth, C. Gwenlan, R. Hall-Wilton, T.W. Jones, M.S. Lightwood, J.H. Loizides[33], B.J. West
Physics and Astronomy Department, University College London, London, United Kingdom [m]

J. Ciborowski[34], R. Ciesielski[35], R.J. Nowak, J.M. Pawlak, B. Smalska[36], J. Sztuk[37], T. Tymieniecka[38], A. Ukleja[38], J. Ukleja, A.F. Żarnecki
Warsaw University, Institute of Experimental Physics, Warsaw, Poland [q]

M. Adamus, P. Plucinski
Institute for Nuclear Studies, Warsaw, Poland [q]

Y. Eisenberg, L.K. Gladilin[39], D. Hochman, U. Karshon
Department of Particle Physics, Weizmann Institute, Rehovot, Israel [c]

D. Kçira, S. Lammers, L. Li, D.D. Reeder, A.A. Savin, W.H. Smith
Department of Physics, University of Wisconsin, Madison, Wisconsin 53706 [n]

A. Deshpande, S. Dhawan, V.W. Hughes, P.B. Straub
Department of Physics, Yale University, New Haven, Connecticut 06520-8121 [n]

S. Bhadra, C.D. Catterall, S. Fourletov, S. Menary, M. Soares, J. Standage
Department of Physics, York University, Ontario, Canada M3J 1P3 [a]

[1] now at Cornell University, Ithaca/NY, USA
[2] on leave of absence at University of Erlangen-Nürnberg, Germany
[3] now at Ministère de la Culture, de L'Enseignement Supérieur et de la Recherche, Luxembourg
[4] supported by the GIF, contract I-523-13.7/97
[5] PPARC Advanced fellow
[6] supported by the Portuguese Foundation for Science and Technology (FCT)
[7] now at Dongshin University, Naju, Korea
[8] now at Max-Planck-Institut für Physik, München/Germany
[9] now at Université Catholique de Louvain, Louvain-la-Neuve/Belgium
[10] now at Northwestern Univ., Evanston/IL, USA
[11] partly supported by the Israel Science Foundation and the Israel Ministry of Science
[12] supported by the Polish State Committee for Scientific Research, grant no. 2 P03B 09322
[13] member of Dept. of Computer Science
[14] now at Fermilab, Batavia/IL, USA
[15] on leave of absence from Cornell Univ., Ithaca/NY, USA
[16] on leave from Argonne National Laboratory, USA
[17] now at DESY group FEB
[18] on leave of absence at Columbia Univ., Nevis Labs., N.Y./USA
[19] now at INFN Perugia, Perugia, Italy
[20] retired
[21] now at Brookhaven National Lab., Upton/NY, USA
[22] now at Mobilcom AG, Rendsburg-Büdelsdorf, Germany
[23] now at Deutsche Börse Systems AG, Frankfurt/Main, Germany
[24] now at Univ. of Oxford, Oxford/UK
[25] also at University of Tokyo
[26] now at LPNHE Ecole Polytechnique, Paris, France
[27] now at IBM Global Services, Frankfurt/Main, Germany
[28] now at National Research Council, Ottawa/Canada
[29] on leave of absence at The National Science Foundation, Arlington, VA/USA
[30] now at Univ. of London, Queen Mary College, London, UK
[31] present address: Tokyo Metropolitan University of Health Sciences, Tokyo 116-8551, Japan
[32] also at Università del Piemonte Orientale, Novara, Italy
[33] supported by Argonne National Laboratory, USA
[34] also at Łódź University, Poland
[35] supported by the Polish State Committee for Scientific Research, grant no. 2 P03B 07222

[36] now at The Boston Consulting Group, Warsaw, Poland
[37] Łódź University, Poland
[38] supported by German Federal Ministry for Education and Research (BMBF), POL 01/043
[39] on leave from MSU, partly supported by University of Wisconsin via the U.S.-Israel BSF

[a] supported by the Natural Sciences and Engineering Research Council of Canada (NSERC)

[b] supported by the German Federal Ministry for Education and Research (BMBF), under contract numbers HZ1GUA 2, HZ1GUB 0, HZ1PDA 5, HZ1VFA 5

[c] supported by the MINERVA Gesellschaft für Forschung GmbH, the Israel Science Foundation, the U.S.-Israel Binational Science Foundation, the Israel Ministry of Science and the Benozyio Center for High Energy Physics

[d] supported by the German-Israeli Foundation, the Israel Science Foundation, and by the Israel Ministry of Science

[e] supported by the Italian National Institute for Nuclear Physics (INFN)

[f] supported by the Japanese Ministry of Education, Science and Culture (the Monbusho) and its grants for Scientific Research

[g] supported by the Korean Ministry of Education and Korea Science and Engineering Foundation

[h] supported by the Netherlands Foundation for Research on Matter (FOM)

[i] supported by the Polish State Committee for Scientific Research, grant no. 620/E-77/SPUB-M/DESY/P-03/DZ 247/2000-2002

[j] partially supported by the German Federal Ministry for Education and Research (BMBF)

[k] supported by the Fund for Fundamental Research of Russian Ministry for Science and Education and by the German Federal Ministry for Education and Research (BMBF)

[l] supported by the Spanish Ministry of Education and Science through funds provided by CICYT

[m] supported by the Particle Physics and Astronomy Research Council, UK

[n] supported by the US Department of Energy

[o] supported by the US National Science Foundation

[p] supported by the Polish State Committee for Scientific Research, grant no. 112/E-356/SPUB-M/DESY/P-03/DZ 301/2000-2002, 2 P03B 13922

[q] supported by the Polish State Committee for Scientific Research, grant no. 115/E-343/SPUB-M/DESY/P-03/DZ 121/2001-2002, 2 P03B 07022

1 Introduction

Studies of deep inelastic scattering (DIS) have played a key role in the development of the Standard Model (SM) and in understanding the structure of nucleons. The HERA $e^{\pm}p$ collider allows the measurement of DIS over a kinematic region that extends to large values of the negative of the four-momentum-transfer squared, Q^2, as well as to low Bjorken x. The SM describes $e^{\pm}p$ neutral current (NC) DIS in terms of the space-like exchange of a virtual photon and a virtual Z boson. When Q^2 is much smaller than the square of the Z-boson mass, M_Z^2, the Z-exchange contribution is negligible. For $Q^2 \sim M_Z^2$, the Z-exchange contribution is comparable to that of photon exchange.

Using data collected during e^+p running from 1994 to 1997, when HERA ran at a centre-of-mass energy, $\sqrt{s}$, of 300 GeV, the ZEUS and H1 collaborations have measured the NC DIS cross section up to Q^2 values as high as $40\,000\,\mathrm{GeV}^2$ [**?**, **?**]. The measured e^+p NC DIS cross sections for Q^2 values larger than $10\,000\,\mathrm{GeV}^2$ are well described at next-to-leading order (NLO) in quantum chromodynamics (QCD) by the SM prediction including both photon- and Z-exchange contributions. The effect of the parity-violating part of the Z exchange to e^+p NC scattering is to decrease the cross section below that expected for photon exchange alone. In e^-p NC DIS, the sign of this contribution is reversed, so that the SM cross section is larger than that expected from pure photon exchange. The comparison of the e^-p with the e^+p NC cross section, therefore, provides a direct test of the electroweak sector of the SM. Cross sections for e^-p NC DIS were reported recently by the H1 collaboration [**?**].

This paper presents the NC e^-p DIS cross-sections $d^2\sigma/dx\,dQ^2$ for $185 < Q^2 < 50\,000\,\mathrm{GeV}^2$ and $0.0037 < x < 0.75$, together with measurements of $d\sigma/dQ^2$, $d\sigma/dx$ and $d\sigma/dy$ for $Q^2 > 200\,\mathrm{GeV}^2$, where $y = Q^2/sx$, neglecting the proton mass. To exhibit the effect of Z-boson exchange, $d\sigma/dx$ is also evaluated for $Q^2 > 10\,000\,\mathrm{GeV}^2$. The cross sections were obtained using the e^-p data collected in 1998/99 at $\sqrt{s} = 318\,\mathrm{GeV}$, corresponding to an integrated luminosity of $(15.9 \pm 0.3)\,\mathrm{pb}^{-1}$. The results are compared to recent ZEUS measurements of the e^+p NC cross sections [**?**] and the parity-violating structure function xF_3 is extracted.

2 Standard Model cross sections

The electroweak Born-level NC DIS unpolarised cross sections for the reactions $e^{\pm}p \to e^{\pm}X$ can be expressed as [**?**, **?**]

$$\frac{d^2\sigma_{\mathrm{Born}}(e^{\pm}p)}{dx\,dQ^2} = \frac{2\pi\alpha^2}{xQ^4}\left[Y_+F_2\left(x,Q^2\right) \mp Y_-xF_3\left(x,Q^2\right) - y^2F_L\left(x,Q^2\right)\right] , \qquad (1)$$

where α is the fine-structure constant and $Y_\pm \equiv 1 \pm (1-y)^2$. At leading order (LO) in QCD, the structure functions F_2 and xF_3 can be written as products of electroweak couplings and parton density functions (PDFs) as follows:

$$F_2 = \tfrac{1}{2} x \sum_f \left[(V_f^L)^2 + (V_f^R)^2 + (A_f^L)^2 + (A_f^R)^2 \right] (q_f + \bar{q}_f) \; ,$$

$$xF_3 = \; x \sum_f \left[V_f^L A_f^L - V_f^R A_f^R \right] (q_f - \bar{q}_f) \; ,$$

where $xq_f(x,Q^2)$ are the quark and $x\bar{q}_f(x,Q^2)$ the anti-quark PDFs, and f runs over the five quark flavours $u, ..., b$. The functions V_f and A_f can be written in terms of the fermion vector and axial-vector couplings as

$$V_f^L(Q^2) = e_f - (v_e + a_e)\, v_f \; \chi_Z(Q^2) \; ,$$

$$V_f^R(Q^2) = e_f - (v_e - a_e)\, v_f \; \chi_Z(Q^2) \; ,$$

$$A_f^L(Q^2) = \quad - (v_e + a_e)\, a_f \; \chi_Z(Q^2) \; ,$$

$$A_f^R(Q^2) = \quad - (v_e - a_e)\, a_f \; \chi_Z(Q^2) \; ,$$

where L and R refer to the left- and right-handed quark states, respectively. The weak couplings $a_{e,f}$ and $v_{e,f}$ ($a_{e,f} = T^3_{e,f}$ and $v_{e,f} = T^3_{e,f} - 2e_{e,f}\sin^2\theta_W$) are functions of the weak isospin, $T^3_{e,f}$ ($T^3_{e,f} = \frac{1}{2}$ ($-\frac{1}{2}$) for ν, u (e, d)), and the weak mixing angle, θ_W($\sin^2\theta_W = 0.232$ [**?**]), e_f is the electric charge of the quark in units of the positron charge and χ_Z is given by

$$\chi_Z(Q^2) = \frac{1}{4\sin^2\theta_W \cos^2\theta_W} \; \frac{Q^2}{Q^2 + M_Z^2} \; .$$

The reduced cross section, $\tilde{\sigma}$, is defined as

$$\tilde{\sigma} = \frac{x\, Q^4}{2\pi\alpha^2 Y_+} \; \frac{d^2\sigma_{\rm Born}}{dx\, dQ^2} \; . \tag{2}$$

All cross-section calculations presented in this paper have been performed using NLO QCD, in which F_L is non-zero [**?**]. These calculations predict that the contribution of F_L to $d^2\sigma_{\rm Born}/dx\, dQ^2$ is approximately 1.3%, averaged over the kinematic range considered in this paper. However, in the region of small x, near $Q^2 = 200\,{\rm GeV}^2$, the F_L contribution to the cross section can be as large as 10%.

3 The ZEUS experiment at HERA

HERA accelerates electrons to an energy of $E_e = 27.5\,{\rm GeV}$ and protons to an energy of $E_p = 920\,{\rm GeV}$, yielding $\sqrt{s} = 318\,{\rm GeV}$. The inter-bunch spacing in the electron and

proton beams is 96 ns. In normal running, some bunches in both the electron and the proton rings are left empty (pilot bunches). The pilot bunches are used to study the single-beam backgrounds.

A detailed description of the ZEUS detector can be found elsewhere [**?**]. A brief outline of the components that are most relevant for this analysis is given below.

The high-resolution uranium–scintillator calorimeter (CAL) [**?**] consists of three parts: the forward (FCAL), the barrel (BCAL) and the rear (RCAL) calorimeters. Each part is subdivided into towers and each tower is longitudinally segmented into one electromagnetic section (EMC) and either one (in RCAL) or two (in BCAL and FCAL) hadronic sections (HAC). The smallest subdivision of the calorimeter is called a cell. The CAL energy resolutions, measured under test-beam conditions, are $\sigma(E)/E = 0.18/\sqrt{E}$ for electrons and $\sigma(E)/E = 0.35/\sqrt{E}$ for hadrons (E in GeV). The timing resolution of the CAL is ~ 1 ns for energy deposits greater than 4.5 GeV.

Presampler detectors are mounted in front of the CAL. They consist of scintillator tiles matching the calorimeter towers and measure signals from particle showers created by interactions in the material lying between the interaction point and the calorimeter.

Charged particles are tracked in the central tracking detector (CTD) [**?**], which operates in a magnetic field of 1.43 T provided by a thin superconducting coil. The CTD consists of 72 cylindrical drift chamber layers, organised in 9 superlayers covering the polar-angle[1] region $15^\circ < \theta < 164^\circ$. The transverse-momentum resolution for full-length tracks is $\sigma(p_t)/p_t = 0.0058\,p_t \oplus 0.0065 \oplus 0.0014/p_t$, with p_t in GeV.

The RCAL is instrumented with a layer of $3 \times 3\,\mathrm{cm}^2$ silicon-pad detectors at a depth of 3.3 radiation lengths. This hadron-electron separator (HES) [**?**] is used to improve the electron angle measurements.

The luminosity is measured using the Bethe-Heitler reaction $ep \to e\gamma p$ [**?**]. The resulting small-angle photons are measured by the luminosity monitor, a lead-scintillator calorimeter placed in the HERA tunnel 107 m from the interaction point in the electron beam direction.

[1] The ZEUS coordinate system is a right-handed Cartesian system, with the Z axis pointing in the proton beam direction, referred to as the "forward direction", and the X axis pointing left towards the centre of HERA. The coordinate origin is at the nominal interaction point. The pseudorapidity is defined as $\eta = -\ln\left(\tan\frac{\theta}{2}\right)$, where the polar angle, θ, is measured with respect to the proton beam direction.

4 Monte Carlo simulation

Monte Carlo (MC) simulations were used to evaluate the efficiency for selecting events, to determine the accuracy of the kinematic reconstruction, to estimate the background rate, and to extrapolate the measured cross sections to the full kinematic range. A sufficient number of events was generated to ensure that statistical errors from the MC samples are negligible in comparison to those of the data. The MC samples were normalised to the total integrated luminosity of the data.

Events from NC DIS were simulated including radiative effects, using the HERACLES 4.6.1 [**?**] program with the DJANGOH 1.1 [**?**] interface to the hadronisation programs and using CTEQ5D [**?**] PDFs. In HERACLES, $\mathcal{O}(\alpha)$ electroweak corrections for initial- and final-state radiation, vertex and propagator corrections and two-boson exchange are included. The colour-dipole model of ARIADNE 4.10 [**?**] was used to simulate the $\mathcal{O}(\alpha_S)$ plus leading-logarithmic corrections to the quark-parton model. As a systematic check, the MEPS model of LEPTO 6.5 [**?**] was used. Both programs use the Lund string model of JETSET 7.4 [**?**] for the hadronisation. Diffractive events, characterised by having no particle production between the current jet and the proton remnant, were generated using RAPGAP 2.08/06 [**?**] and appropriately mixed with the non-diffractive NC DIS sample. The contribution of diffractive events, originally generated with the same x-Q^2 distribution as non-diffractive events, was obtained by fitting the $\eta_{\max}$ distribution[2] of the data with a linear combination of non-diffractive and diffractive MC samples while maintaining the overall normalisation [**?**]. The fit was carried out in each of the x-Q^2 bins used in the measurement of the double-differential cross section (see Section 9.1). The fitted fractions exhibited no dependence on Q^2 and an exponential function was used to parameterise the x dependence. The diffractive fraction falls from 10% at $x = 0.005$ to 2% at $x = 0.05$. Photoproduction (PHP) backgrounds, including both direct and resolved processes, were simulated at LO using HERWIG 6.1 [**?**].

The ZEUS detector response was simulated using a program based on GEANT 3.13 [**?**]. The generated events were passed through the detector simulation, subjected to the same trigger requirements as the data and processed by the same reconstruction and analysis programs.

The vertex distribution in data is a crucial input to ensure the accuracy of the evaluation of the event-selection efficiency of the MC. The shape of the Z-vertex distribution was determined from a sample of NC DIS events for which the event-selection efficiency was independent of Z.

[2] The quantity $\eta_{\max}$ is defined as the pseudorapidity of the CAL energy deposit with the lowest polar angle and an energy above 400 MeV.

5 Event characteristics and kinematic reconstruction

Neutral current events with $Q^2 > 200\,\mathrm{GeV}^2$ are characterised by the presence of a high-energy isolated electron. Many of these electrons have an energy close to the beam energy and are scattered into the RCAL. As Q^2 increases, the scattered electrons are produced with higher energies, up to several hundred GeV, and at smaller polar angles, so that they are measured in the BCAL or the FCAL.

The variables δ, P_T and E_T are used in the event selection. The quantity δ is defined by

$$\delta \equiv \sum_i (E - p_Z)_i = \sum_i (E_i - E_i \cos\theta_i) \ , \tag{3}$$

where the sum runs over all calorimeter energy deposits E_i (uncorrected in the trigger but corrected in the offline analysis, as discussed below) with polar angles θ_i. Conservation of energy and longitudinal momentum, p_z, requires $\delta = 2E_e = 55\,\mathrm{GeV}$ if all final-state particles are detected and perfectly measured. Undetected particles that escape through the forward beam hole have a negligible effect on δ. However, particles lost through the rear beam hole, as in the case of PHP, where the electron emerges at very small scattering angles, or in events with an initial-state bremsstrahlung photon, can lead to a substantial reduction in δ.

The net transverse momentum, P_T, and the transverse energy, E_T, are defined by

$$\begin{aligned} P_T^2 = \ & P_X^2 + P_Y^2 = \left(\sum_i E_i \sin\theta_i \cos\phi_i\right)^2 + \left(\sum_i E_i \sin\theta_i \sin\phi_i\right)^2 , \\ E_T = & \sum_i E_i \sin\theta_i \ , \end{aligned} \tag{4}$$

where ϕ_i is the azimuthal angle, and the sums run over all energy deposits in the calorimeter.

The CAL energy deposits were separated into those associated with the scattered electron and all other energy deposits. The sum of the latter is referred to as the hadronic energy. The spatial distribution of the hadronic energy, together with the reconstructed vertex position, were used to evaluate the hadronic polar angle, γ_h, which, in the naive quark-parton model, is the polar angle of the struck quark.

The reconstruction of x, Q^2 and y was performed using the double angle (DA) method [**?**].

The DA estimators are given by

$$Q^2_{\rm DA} = 4E_e^2 \frac{\sin\gamma_h(1+\cos\theta_e)}{\sin\gamma_h + \sin\theta_e - \sin(\gamma_h+\theta_e)} \ ,$$

$$x_{\rm DA} = \frac{E_e}{E_p}\frac{\sin\gamma_h + \sin\theta_e + \sin(\gamma_h+\theta_e)}{\sin\gamma_h + \sin\theta_e - \sin(\gamma_h+\theta_e)} \ ,$$

$$y_{\rm DA} = \frac{\sin\theta_e(1-\cos\gamma_h)}{\sin\gamma_h + \sin\theta_e - \sin(\gamma_h+\theta_e)} \ ,$$

where θ_e is the polar angle of the scattered electron.

The DA method is insensitive to uncertainties in the overall energy scale of the calorimeter. However, it is sensitive to initial-state QED radiation and, in addition, an accurate simulation of the hadronic final state is necessary.

The relative resolution in Q^2 was 3% over the entire kinematic range covered. The relative resolution in x varied from 15% in the lowest Q^2 bins to 4% in the highest Q^2 bins. The relative resolution in y was 10% in the lowest Q^2 bins, decreasing to 1% for high y values in the highest Q^2 bins (see Section 9.1).

In the event selection, y calculated using the electron method (y_e) and the Jacquet-Blondel method [**?**] ($y_{\rm JB}$) were also used. These variables are defined by

$$y_e = 1 - \frac{E'_e}{2E_e}\,(1-\cos\theta_e) \ ,$$

$$y_{\rm JB} = \frac{\delta_h}{2E_e} \ ,$$

where E'_e is the energy of the scattered electron and δ_h was calculated from Eq. (3) using only the hadronic energy.

6 Electron reconstruction

6.1 Electron identification

In order to identify and reconstruct the scattered electron, an algorithm that combines calorimeter and CTD information was used [**?**]. The algorithm starts by identifying CAL clusters that are topologically consistent with an electromagnetic shower. Each cluster had to have an energy of at least 10 GeV and, if the electron candidate fell within the acceptance of the CTD, a track was required that, when extrapolated, had to pass within 10 cm of a cluster centre at the shower maximum. Such a track is referred to as a matched

track. An electron candidate was considered to lie within the CTD acceptance if a matched track from the reconstructed event vertex traversed at least four of the nine superlayers of the CTD. For the nominal interaction point, i.e. $Z = 0$, this requirement corresponds to the angular range of $23^\circ < \theta_e < 156^\circ$.

Monte Carlo studies showed that the overall efficiency for finding the scattered electron was about 95% for $E'_e \geq 10\,\mathrm{GeV}$ and $Q^2 < 15\,000\,\mathrm{GeV}^2$, decreasing to about 85% for $Q^2 > 30\,000\,\mathrm{GeV}^2$. The electron identification efficiency was checked with a data sample of NC DIS events selected using independent requirements such as high E_T in the trigger and an isolated high-p_t track associated with the scattered electron. The efficiency curves from data and MC simulation agreed to better than 0.5%. An alternative electron-finding algorithm [**?**] was also used: differences in the measured cross sections were negligible.

6.2 Electron-energy determination

The scattered-electron energy was determined from the calorimeter deposit since, above 10 GeV, the calorimeter energy resolution is better than the momentum resolution of the CTD. The measured energy was corrected for the energy lost in inactive material in front of the CAL. The presampler was used in the RCAL, while in the B/FCAL a detailed material map was used [**?**]. To render the energy response uniform across the face of the calorimeter, corrections, obtained by smoothing the non-uniform response functions in data and the MC simulation, were used [**?**]. The corrections were determined separately for the BCAL [**?**] and the RCAL [**?**]. Too few electrons were scattered into the FCAL for such a correction to be derived.

After applying the corrections described above, the electron-energy resolution was 10% at $E'_e = 10\,\mathrm{GeV}$ falling to 5% for $E'_e > 20\,\mathrm{GeV}$. The scale uncertainty on the energy of the scattered electron detected in the BCAL was $\pm 1\%$. For electrons detected in the RCAL, the scale uncertainty was $\pm 2\%$ at 8 GeV, falling linearly to $\pm 1\%$ for electrons with energies of 15 GeV and above [**?**]. A scale uncertainty of $\pm 3\%$ was assigned to electrons reconstructed in the FCAL.

6.3 Determination of the electron polar angle

The polar angle of the scattered electron can be determined either from the cluster position within the calorimeter using the reconstructed event vertex, or from the polar angle of the track matched to the cluster. Studies [**?**] showed that, inside the acceptance of the CTD, the angular resolution for tracks is superior to that for calorimeter clusters. Hence, in the CTD acceptance region, which contains 98.8% of the events, θ_e was determined

from the track. For candidates outside this region, the position of the cluster was used together with the event vertex.

To determine the CAL alignment, the positions of the calorimeter cell boundaries were obtained by using the energy-deposition pattern of electron tracks extrapolated into the CAL. This allowed the BCAL to be aligned in Z (ϕ) with respect to the CTD to $\pm 0.3\,\mathrm{mm}$ ($\pm 0.6\,\mathrm{mrad}$) [**?**]. For the alignment of the RCAL, the position of the extrapolated track was compared to that determined by the HES [**?**]. The precision of the alignment was $\pm 0.3\,\mathrm{mm}$ ($\pm 0.6\,\mathrm{mm}$) in X (Z) and $\pm 0.9\,\mathrm{mrad}$ in ϕ. In all cases, the precision is sufficient to render the resulting systematic uncertainties on the cross sections negligible.

The resolution in θ_e was obtained by comparing the MC-generated angle to that obtained after applying the detector simulation, reconstruction and correction algorithms. The resulting resolution for electrons outside the CTD acceptance was $\pm 5\,\mathrm{mrad}$ in the RCAL and $\pm 2\,\mathrm{mrad}$ in the FCAL. For tracks inside the CTD acceptance, the resolution was $\pm 3\,\mathrm{mrad}$.

7 Reconstruction of the hadronic system

7.1 Hadronic-energy determination

The hadronic-energy deposits were corrected for energy loss in the material between the interaction point and the calorimeter using the material maps implemented in the detector-simulation package.

After applying all corrections, the measured resolution for the hadronic transverse momentum, p_T^{had}, was about 13% (11%) at $p_T^{\mathrm{had}} = 20\,\mathrm{GeV}$ in BCAL (FCAL), decreasing to 8% (7.5%) at $p_T^{\mathrm{had}} = 60\,\mathrm{GeV}$. The uncertainties in the hadronic energy scales of the FCAL and the BCAL were $\pm 1\%$, while for the RCAL the uncertainty was $\pm 2\%$ [**?**].

7.2 Determination of the hadronic polar angle, γ_h

The angle γ_h is given by [**?**]

$$\cos\gamma_h = \frac{P_{T,h}^2 - \delta_h^2}{P_{T,h}^2 + \delta_h^2},$$

where $P_{T,h}^2$ was calculated from Eq. (4) using only the hadronic energy. Particles interacting in the material between the primary vertex and the CAL generate energy deposits that bias the reconstructed value of γ_h. To minimise this bias, an algorithm was developed

in which CAL clusters with energies below 3 GeV and with polar angles larger than an angle $\gamma_{\max}$ were removed [**?**]. The value of $\gamma_{\max}$ was derived from a NC MC sample by requiring that the bias in the reconstructed hadronic variables was minimised.

The resolution of γ_h was below 15 mrad for $\gamma_h < 0.2$ rad, increasing to 100 mrad at $\gamma_h \sim 2$ rad. These resolutions dominate the errors on the kinematic variables.

8 Event selection

8.1 Trigger

ZEUS operates a three-level trigger system [**?**]. For the measurements presented in this paper, the first-level trigger required an "OR" of the following:

- a total electromagnetic energy of at least 3.4 GeV in the EMC cells of the RCAL;
- 4.8 GeV in the EMC cells of the BCAL and a "good track", defined as a charged track consistent with emanating from the IP;
- an isolated energy deposit of at least 2 GeV in the EMC section of the RCAL;
- 15 GeV summed over the entire EMC cells of the CAL;
- $E_T'' > 12$ GeV and a good track, where E_T'' is the total transverse energy excluding the two rings of FCAL towers nearest to the forward beampipe.

The E_T'' requirement was designed to tag high-Q^2 events by their large E_T while rejecting beam-gas background. The latter is characterised by large energy deposits at low polar angles. The major requirement at the second trigger level was $\delta + 2E_\gamma > 29$ GeV, where E_γ is the energy measured in the luminosity monitor. This requirement suppresses photoproduction events. Backgrounds were further reduced at the second level by removing events with calorimeter timing inconsistent with an *ep* interaction. At the third level, events were fully reconstructed. The requirements were similar to, but looser than, the offline cuts described below; a simpler and generally more efficient (but less pure) electron finder was used.

The main uncertainty in the trigger chain comes from the first level. The data and MC simulation agree to within $\sim 0.5\%$ and the overall efficiency is close to 100%. Therefore, uncertainties on the measured cross sections coming from the trigger simulation are small.

8.2 Offline selection

The following criteria were applied offline:

- electrons, identified as described in Section 6, were required to satisfy the following criteria:
  - to ensure high purity, the electron was required to have an energy of at least 10 GeV;
  - to reduce background, isolated electrons were selected by requiring that less than 5 GeV, not associated with the scattered electron, be deposited in calorimeter cells inside an η-ϕ cone of radius $R_{\rm cone} = 0.8$ centred on the electron. The quantity $R_{\rm cone}$ is defined as $R_{\rm cone} = \sqrt{(\Delta\phi)^2 + (\Delta\eta)^2}$, where $\Delta\phi$ (in radians) is the azimuthal angle between the CAL energy deposit and the scattered electron and $\Delta\eta$ is the difference in pseudorapidity between the scattered electron and the energy deposit;
  - each electron cluster within the CTD acceptance ($23^\circ \lesssim \theta_e \lesssim 156^\circ$) had to be matched to a track with a momentum, $p_{\rm trk}$, of at least 5 GeV. The distance of closest approach (DCA) of the extrapolated track to the centre of the CAL cluster had to be less than 10 cm;
  - for electrons outside of the forward tracking acceptance of the CTD ($\theta_e \lesssim 23^\circ$), the tracking requirement in the electron selection was replaced by a cut on the transverse momentum of the electron, $p_t^e > 30$ GeV;
  - for electrons outside the backward tracking acceptance of the CTD ($\theta_e \gtrsim 156^\circ$), no track was required;
  - a fiducial-volume cut was applied to the electron. It excluded the upper part of the central RCAL area ($20 \times 80\,{\rm cm}^2$), which is occluded by the cryogenic supply for the solenoid magnet, as well as the transition regions between the three parts of the CAL, corresponding to scattered-electron polar angles of $35.6^\circ < \theta_e < 37.3^\circ$ and $128.2^\circ < \theta_e < 140.2^\circ$;
- to ensure that event quantities were accurately determined, a reconstructed vertex with $-50 < Z < 50$ cm was required, a range consistent with the ep interaction region. A small fraction of the proton current was contained in satellite bunches, which were separated by ± 4.8 ns with respect to the nominal bunch-crossing time, resulting in some of the ep interactions occurring ± 72 cm from the nominal interaction point. This cut rejects ep events from these regions;
- to suppress PHP events, in which the scattered electron escaped through the beam hole in the RCAL, δ was required to be greater than 38 GeV. This cut also reduces the number of events with initial-state QED radiation. The requirement $\delta < 65$ GeV

removed "overlay" events in which a normal DIS event coincided with additional energy deposits in the RCAL from some other source. For electrons outside the forward tracking acceptance of the CTD, the lower δ cut was raised to 44 GeV;

- to reduce further the background from PHP, y_e was required to satisfy $y_e < 0.95$;
- the net transverse momentum, P_T, is expected to be close to zero for true NC events and was measured with an error approximately proportional to $\sqrt{E_T}$. To remove cosmic rays and beam-related background, $P_T/\sqrt{E_T}$ was required to be less than $4\sqrt{\text{GeV}}$;
- to reduce the contribution from QED radiative corrections, elastic Compton scattering events ($ep \to e\gamma p$) were removed. This was done using an algorithm that searched for an additional photon candidate and discarded the event if the sum of the energies associated with the electron and photon candidates was within 2 GeV of the total energy in the calorimeter;
- in events with low γ_h, a large amount of energy is deposited near the inner edges of the FCAL or escapes through the forward beampipe. As the MC simulation of this forward energy flow is somewhat uncertain, events for which γ_h, extrapolated to the FCAL surface, lay within a circle of 20 cm around the forward beam line were removed. For an interaction at the nominal interaction point, this circle cut corresponds to a lower γ_h cut of 90 mrad;
- the kinematic range over which the MC simulation is valid does not extend to very low y at high x. To avoid these regions of phase space, $y_{\text{JB}}(1 - x_{\text{DA}})^2$ was required to be greater than 0.004 [**?**].

A total of 38 411 events with $Q^2_{\text{DA}} > 185\,\text{GeV}^2$ satisfied the above criteria. Distributions from data and the sum of the signal and PHP-background MC samples are compared in Fig. 1. Good agreement between data and MC simulation is seen over the full range of most variables. Disagreements between data and MC simulation occur in the region of the kinematic peak ($E'_e \approx E_e$) in the electron energy distribution, at high and low values of the momentum of the electron track, p_{trk}, and in the peak region of the distribution of δ. The differences suggest that there are simulation errors in some aspects of either or both the fragmentation and the detector response. The uncertainties caused by these disagreements were included in the systematic uncertainties (see Section 9.2).

The PHP background averages $\sim 0.3\%$ over the kinematic range covered, rising to $\sim 1.3\%$ at high y. Background from prompt-photon events is negligible [**?**]. An upper limit to the background associated with non-ep collisions is given by the absence of any events from pilot bunches. Taking into account the relative currents in the pilot and colliding bunches yields a 90% C.L. upper limit of 70 events. Backgrounds from sources not related to ep collisions were therefore neglected.

9 Results

9.1 Binning, acceptance and cross-section determination

The bin sizes used for the determination of the single- and double-differential cross sections were chosen commensurate with the resolutions. Figure 2 shows the kinematic region used in extracting the $e^- p$ double-differential cross section. The number of events per bin decreases from $\sim 1\,800$ in the lowest Q^2 bins to four in the bin at the highest Q^2 and x. The efficiency, defined as the number of events generated and reconstructed in a bin divided by the number of events that were generated in that bin, varied between 50% and 80%, apart from the region between the R/BCAL at $\theta_e = 2.25\,\text{rad}$. The purity, defined as the number of events reconstructed and generated in a bin divided by the total number of events reconstructed in that bin, ranged from 50% to 80%. The acceptance, $\mathcal{A}$, listed in the tables, is defined as the efficiency divided by the purity.

The value of the cross section at a fixed point within a bin was obtained from the ratio of the number of observed events, after background subtraction, to the number of events estimated from the MC simulation in that bin, multiplied by the appropriate cross section obtained from Eq. (2) using the CTEQ5D PDFs. In this way, the $d\sigma/dQ^2$ and $d\sigma/dx$ measurements were extrapolated to the full range of y and corrected for initial- and final-state radiation. Using the ZEUS NLO QCD (ZEUS-S) fit [**?**] in the extraction of the cross sections instead of CTEQ5D typically changed the single-differential cross sections by less than $\pm 1\%$; only in the highest Q^2 bins was the effect as large as 3%. The change in the double-differential cross section was typically below $\pm 1\%$ and increased to $\pm 2\%$ only in the upper Q^2 bins at high x.

The statistical uncertainties on the cross sections were calculated, using Poisson statistics, from the numbers of events observed in the bins, taking into account the statistical uncertainty from the MC simulations.

9.2 Systematic uncertainties

Systematic uncertainties associated with deficiencies in the simulation were estimated by re-calculating the cross sections after tuning the MC simulation. Values of the event-selection cuts were varied where this method was not applicable. The positive and negative deviations from the nominal cross-section values were added in quadrature separately to obtain the total positive and negative systematic uncertainty. The uncertainty on the luminosity of the combined 1998–99 $e^- p$ sample of 1.8% was not included in the total systematic uncertainty. The other uncertainties are discussed in detail below.

9.2.1 Uncorrelated systematic uncertainties

The following systematic uncertainties exhibit no bin-to-bin correlations:

- variation of the electron-energy resolution in the MC simulation — the effect on the cross sections of changing the CAL energy resolution for the scattered electron in the MC by ±1% was negligible over nearly the full kinematic range. The effect increased to about ±1% only for bins at high y and for double-differential bins in the upper Q^2 range;
- electron angle — differences between data and MC simulation in the electron scattering angle due to uncertainties in the simulation of the CTD were at most ±1 mrad. Typically, the variations were below ±1%; the effect increased to as much as ±2% in only a few double-differential bins.

  For electrons outside the forward acceptance of the CTD, the FCAL position was varied by ±3 mm in X, Y and Z, covering the uncertainty on the FCAL alignment. Typically, the changes in the cross sections were below ±1% and reached ±2% in only a few double-differential bins at high x;
- hadronic angle — the uncertainty associated with the reconstruction of γ_h was investigated by varying the calorimeter-energy scale for the hadronic final state [**?**] and by varying the $\gamma_{\max}$ parameter in the correction to the hadronic energy given in Section 7.2 in a range for which the reconstruction of γ_h remains close to optimal. This resulted in a systematic uncertainty in the single-differential cross sections of less than ±1% in most bins, increasing to about ±2% in individual bins. For the double-differential bins, the effect was generally below ±2% at low and medium Q^2, occasionally reaching ±4%. In the highest Q^2 region, the effect was as large as ±7%;
- FCAL circle cut — the cut at 20 cm was varied by ±3 cm. The resulting changes in the cross sections were typically below ±1%. Only for the highest x bins of the double-differential cross section did the effect increase to ±6% and in two bins at $Q^2 = 1\,200\,\mathrm{GeV}^2$ and $1\,500\,\mathrm{GeV}^2$ ($x = 0.4$) to −17% and +40%, respectively;
- background estimation — systematic uncertainties arising from the normalisation of the PHP background were estimated by doubling and halving the background predicted by the MC simulation, resulting in negligible changes in the single-differential cross sections over the full kinematic range and small variations of at most ±1% in the double-differential bins;
- variation of selection thresholds — the DCA cut was lowered from 10 cm to 8 cm. The uncertainties in the cross sections associated with this changes were below ±2% over the full kinematic range, except for two double-differential bins at high x, where the effect reached −6%.

The upper δ cut at 65 GeV was varied by ± 2 GeV. The effect on the cross sections was generally below $\pm 1\%$ but became as large as $\pm 15\%$ in a few bins.

The $P_T/\sqrt{E_T}$ cut was varied by $\pm 1\sqrt{\text{GeV}}$. The cross-section uncertainties were below about $\pm 1\%$ over the full kinematic range;

- diffractive contribution — the fraction of diffractive events was varied within the errors determined by the fit described in Section 4. The resulting uncertainties were typically below $\pm 1\%$, rising to about $\pm 2\%$ at high y.

9.2.2 Correlated systematic uncertainties

The following systematic uncertainties were found to be correlated bin to bin:

- $\{\delta_1\}$ electron-energy scale — the uncertainty in the electron-energy scale (as described in Section 6) resulted in systematic variations in the cross sections of $\pm 2\%$ at high y and in negligible uncertainties elsewhere;
- $\{\delta_2\}$ background estimation — systematic uncertainties arising from the simulation of the PHP background were estimated by reducing the cut on y_e to $y_e < 0.9$. The resulting changes in the cross sections were typically below $\pm 2\%$; only in the highest-Q^2 region at low x did the effect increase to $\pm 13\%$;
- $\{\delta_3\}$ variation of selection thresholds (I) — varying the electron-isolation requirement by ± 2 GeV caused a negligible systematic uncertainty in the cross sections at the lower end of the Q^2 and y range, up to $\pm 2\%$ for the medium Q^2 and high y bins and up to $\pm 5\%$ in the highest Q^2 bins;
- $\{\delta_4\}$ variation of selection thresholds (II) — varying the p_{trk} requirement by ± 5 GeV resulted in variations of the cross sections by at most $\pm 2\%$ over nearly the full kinematic range, except in a few double-differential bins where it became as high as $\pm 8\%$;
- $\{\delta_5\}$ vertex distribution — the uncertainty arising from the limited knowledge of the shape of the distribution in the Z coordinate of the event vertex was obtained by varying the contribution of events from the satellite bunches, visible as small peaks for $|Z| > 50$ cm in Fig. 1e), by $+40\%$ and -8% in the MC simulation, as suggested by comparison with data. The effect on the cross sections was at most about $\pm 1\%$;
- $\{\delta_6\}$ uncertainty in the parton-shower scheme — a comparison of the description of the hadronic energy flow in data with the expectations of ARIADNE and the MEPS model of LEPTO was made. ARIADNE gave a slightly better description of the data. However, small differences with respect to the data were observed for both models, particularly in the energy flow between the current jet and the target remnant. The

effects on the cross sections were typically below $\pm 2\%$, reaching as much as $\pm 6\%$ in only a few bins.

9.3 Single-differential cross sections

The single-differential cross-section $d\sigma/dQ^2$ is shown in Fig. 3a) and tabulated in Table 1. The systematic uncertainties are collected in Table 2. The ratio of $d\sigma/dQ^2$ to ZEUS-S, displayed in Fig. 3b), shows that the SM gives a good description of the data. Note that the ZEUS-S fit did not use the data presented in this paper. The cross-sections $d\sigma/dx$ and $d\sigma/dy$ for $Q^2 > 200\,\mathrm{GeV}^2$ are shown in Fig. 4 and are tabulated in Tables 3 and 5 (systematic uncertainties are listed in Tables 4 and 6). The SM cross sections, evaluated using the ZEUS-S PDFs, again give a good description of the data. The plots also contain the SM predictions using the CTEQ5D [**?**] and MRST99 [**?**] PDFs.

The Z-boson-exchange contribution to NC DIS is clearly seen in Fig. 5, which compares $d\sigma/dx$ for e^+p [**?**] and e^-p scattering for $Q^2 > 10\,000\,\mathrm{GeV}^2$. The e^-p cross section is significantly larger than the e^+p cross section. This is due to the parity-violating part of the Z-exchange contribution enhancing the e^-p NC DIS cross section and suppressing the e^+p NC DIS cross section compared to pure photon exchange. The lines for pure photon exchange are different because of the different centre-of-mass energies at which the e^+p and e^-p data sets were taken.

9.4 Reduced cross section

The reduced cross section, $\tilde{\sigma}(e^-p)$, tabulated in Tables 7 and 12 (systematic uncertainties are listed in Tables 13 and 18), is shown in Fig. 6 as a function of x for fixed Q^2. The rise of $\tilde{\sigma}(e^-p)$ at fixed Q^2 as x decreases reflects the strong rise of F_2 [**?**]. The SM, evaluated with the ZEUS-S PDFs, gives a good description of the data.

Figure 7 shows the reduced cross section plotted as a function of Q^2 at several values of x. The plot also contains the ZEUS measurement of $\tilde{\sigma}(e^+p)$ [**?**], based on data collected at $\sqrt{s} = 300\,\mathrm{GeV}$. For Q^2 values below $\sim 3\,000\,\mathrm{GeV}^2$, the e^+p and e^-p cross sections are nearly equal. At higher Q^2, $\tilde{\sigma}(e^-p)$ is greater than $\tilde{\sigma}(e^+p)$ as expected from Z-boson exchange.

9.5 The xF_3 structure function and electroweak analysis

The parity-violating structure function, xF_3, was obtained, using Eqs. (1) and (2), by subtracting the respective reduced cross sections. Since the $\tilde{\sigma}(e^+p)$ cross section was

measured at a centre-of-mass energy of 300 GeV [?], xF_3 was determined by evaluating

$$xF_3 = \left(\frac{Y_-^{300}}{Y_+^{300}} + \frac{Y_-^{318}}{Y_+^{318}} \right)^{-1} \left(\tilde{\sigma}(e^-p) - \tilde{\sigma}(e^+p) \right) - \Delta_{F_L} \ , \tag{5}$$

where the superscripts '300' and '318' denote the different centre-of-mass energies. The term Δ_{F_L} in Eq. (5) is non-zero because of the different centre-of-mass energies at which the e^+p and e^-p data were collected. The relative size of Δ_{F_L}, computed at NLO in QCD, is less than 1% over most of the kinematic range in which xF_3 is presented and is neglected.

To reduce statistical fluctuations, several bins used in the measurement of the double-differential cross section were combined. Figure 8a) shows xF_3 at fixed values of Q^2 as a function of x, whereas Fig. 8b) shows xF_3 at fixed values of x as a function of Q^2. The measured values are tabulated in Table 19. Since the statistical errors dominate the uncertainty, systematic uncertainties were assumed to be uncorrelated between the e^+p and the e^-p data sets. The luminosity errors have been included in the total systematic uncertainty on the most conservative assumption that they are completely anti-correlated. The expectation of the SM, evaluated with the ZEUS-S PDFs, gives a good description of the data.

To compare the present measurement of xF_3 to that obtained at lower Q^2 in fixed-target experiments, it is convenient to use two structure functions $xG_3(x, Q^2)$ and $xH_3(x, Q^2)$ [?] as follows:

$$xF_3 = -a_e \chi_Z \, xG_3 + 2 v_e a_e \chi_Z^2 \, xH_3 \ .$$

The term containing xG_3 arises from γ-Z interference, while the xH_3 term arises purely from Z exchange. The xH_3 term is negligible in comparison to the xG_3 term because the coefficient multiplying xH_3 contains the vector coupling of the electron, $v_e = -0.054$, and xH_3 itself is less than half the size of xG_3. At fixed x, xG_3 depends weakly on Q^2 [?, ?]. For example, according to the ZEUS-S PDFs, at $x = 0.25$, xG_3 varies from 0.46 at $Q^2 = 100\,\text{GeV}^2$ to 0.37 at $Q^2 = 10\,000\,\text{GeV}^2$.

Each value of xF_3 was used to obtain an estimate of xG_3 by evaluating

$$xG_3 \cong \frac{xF_3}{[-a_e \chi_Z]} \ .$$

The weak Q^2 dependence of xG_3 was accounted for by extrapolating each xG_3 value to $Q^2 = 1\,500\,\text{GeV}^2$ using ZEUS-S PDFs. In order to reduce statistical fluctuations, xG_3 values from different bins with the same x were combined by computing the weighted mean of the individual estimates of xG_3. Since the errors are not symmetric, the mean of the upper and lower statistical error was used as the weight in this calculation.

The result of the above procedure is shown in Fig. 9. This figure also shows the results obtained by the BCDMS collaboration [**?**], which were extracted over the kinematic range $40 < Q^2 < 180\,\mathrm{GeV}^2$ and $0.2 < x < 0.7$ from NC muon-carbon scattering. The value of xG_3 extracted by the BCDMS collaboration is therefore the average of xG_3 for the proton and the neutron, since the target nucleus is isoscalar. Figure 9 shows xG_3 evaluated for ep scattering at $Q^2 = 1\,500\,\mathrm{GeV}^2$ and for μN scattering at $Q^2 = 100\,\mathrm{GeV}^2$ using the ZEUS-S PDFs. The difference between the theoretical predictions for ep and μN scattering, evaluated with ZEUS-S PDFs, is small and the BCDMS data agree well with the present measurement. The ZEUS data extend the measurement of xG_3 down to $x = 0.05$.

10 Summary

The cross sections for neutral current deep inelastic scattering, $e^- p \to e^- X$, have been measured using $15.9\,\mathrm{pb}^{-1}$ of data collected with the ZEUS detector during the 1998–99 running periods. The single-differential cross-sections $d\sigma/dQ^2$, $d\sigma/dx$ and $d\sigma/dy$ have been measured for $Q^2 > 200\,\mathrm{GeV}^2$. In order to exhibit the effect of Z-boson exchange, $d\sigma/dx$ has also been measured for $Q^2 > 10\,000\,\mathrm{GeV}^2$. The reduced cross section has been measured in the kinematic range $185 < Q^2 < 50\,000\,\mathrm{GeV}^2$ and $0.0037 < x < 0.75$. The Standard Model predictions, including both γ and Z exchange and using standard parton density functions (ZEUS-S, CTEQ5D and MRST99), are in good agreement with the data.

The parity-violating structure function, xF_3, has been extracted by combining the data presented here with the published ZEUS measurement of the reduced cross section for neutral current $e^+ p$ deep inelastic scattering. The structure function xG_3 has been extracted from the xF_3 measurement and compared to previous results obtained in fixed-target muon-carbon scattering by the BCDMS collaboration. The ZEUS results are in good agreement with the BCDMS measurement and extend the range of x values covered down to $x = 0.05$. The results are also in good agreement with theoretical predictions and, since xF_3 is non-zero, show the presence of Z exchange in the space-like Q^2 region explored by deep inelastic ep scattering.

11 Acknowledgements

The strong support and encouragement of the DESY Directorate have been invaluable. The experiment was made possible by the inventiveness and the diligent efforts of the HERA machine group. The design, construction and installation of the ZEUS detector have been made possible by the ingenuity and dedicated efforts of many people from

inside DESY and from home institutes who are not listed as authors. Their contributions are acknowledged with great appreciation. Special thanks are due to Hannes Jung who helped to modify RAPGAP so that diffractive events could be included in the analysis.

Q^2 range (GeV^2)	Q_c^2 (GeV^2)	$d\sigma/dQ^2$ (pb / GeV^2) measured	$d\sigma/dQ^2$ (pb / GeV^2) SM	N_{obs}	N_{bg}	$\mathcal{A}$
200.0 – 300.0	250	$11.150 \pm 0.105\,^{+0.116}_{-0.153}$	11.220	15360	3.5	0.80
300.0 – 400.0	350	$5.005 \pm 0.073\,^{+0.037}_{-0.085}$	5.022	6474	2.6	0.76
400.0 – 475.7	440	$2.854 \pm 0.061\,^{+0.025}_{-0.049}$	2.890	2737	0.7	0.74
475.7 – 565.7	520	$1.876 \pm 0.048\,^{+0.025}_{-0.031}$	1.924	1850	1.4	0.65
565.7 – 672.7	620	$1.198 \pm 0.038\,^{+0.013}_{-0.023}$	1.251	1184	0.8	0.54
672.7 – 800.0	730	$(8.82 \pm 0.28\,^{+0.10}_{-0.09}) \cdot 10^{-1}$	$8.36 \cdot 10^{-1}$	1215	0.9	0.65
800.0 – 951.4	870	$(5.27 \pm 0.17\,^{+0.08}_{-0.09}) \cdot 10^{-1}$	$5.41 \cdot 10^{-1}$	1171	0.7	0.86
951.4 – 1131.0	1040	$(3.36 \pm 0.12\,^{+0.06}_{-0.04}) \cdot 10^{-1}$	$3.47 \cdot 10^{-1}$	973	0.6	0.93
1131.0 – 1345.0	1230	$(2.15 \pm 0.09\,^{+0.04}_{-0.02}) \cdot 10^{-1}$	$2.28 \cdot 10^{-1}$	751	1.4	0.98
1345.0 – 1600.0	1470	$(1.54 \pm 0.07\,^{+0.02}_{-0.03}) \cdot 10^{-1}$	$1.45 \cdot 10^{-1}$	638	0.8	0.98
1600.0 – 1903.0	1740	$(9.76 \pm 0.48\,^{+0.18}_{-0.16}) \cdot 10^{-2}$	$9.46 \cdot 10^{-2}$	488	0.6	0.96
1903.0 – 2263.0	2100	$(5.34\,^{+0.32}_{-0.30}\,^{+0.09}_{-0.08}) \cdot 10^{-2}$	$5.86 \cdot 10^{-2}$	333	0.6	0.97
2263.0 – 2691.0	2500	$(3.82\,^{+0.25}_{-0.23}\,^{+0.10}_{-0.07}) \cdot 10^{-2}$	$3.75 \cdot 10^{-2}$	283	1.1	0.97
2691.0 – 3200.0	2900	$(2.45\,^{+0.19}_{-0.18}\,^{+0.04}_{-0.03}) \cdot 10^{-2}$	$2.56 \cdot 10^{-2}$	196	0.2	0.97
3200.0 – 4525.0	3800	$(1.39\,^{+0.09}_{-0.08}\,^{+0.03}_{-0.04}) \cdot 10^{-2}$	$1.27 \cdot 10^{-2}$	308	0.4	0.98
4525.0 – 6400.0	5400	$(5.05\,^{+0.44}_{-0.41}\,^{+0.12}_{-0.12}) \cdot 10^{-3}$	$5.08 \cdot 10^{-3}$	157	0.2	0.96
6400.0 – 9051.0	7600	$(2.13\,^{+0.25}_{-0.22}\,^{+0.03}_{-0.04}) \cdot 10^{-3}$	$2.03 \cdot 10^{-3}$	91	0.0	0.93
9051.0 – 12800.0	10800	$(6.0\,^{+1.2}_{-1.0}\,^{+0.3}_{-0.1}) \cdot 10^{-4}$	$7.6 \cdot 10^{-4}$	35	0.0	0.92
12800.0 – 18100.0	15200	$(3.2\,^{+0.8}_{-0.6}\,^{+0.3}_{-0.1}) \cdot 10^{-4}$	$2.7 \cdot 10^{-4}$	25	0.0	0.90
18100.0 – 25600.0	21500	$(7.1\,^{+3.5}_{-2.5}\,^{+0.4}_{-0.4}) \cdot 10^{-5}$	$8.3 \cdot 10^{-5}$	8	0.0	0.93
25600.0 – 36200.0	30400	$(2.0\,^{+2.0}_{-1.1}\,^{+0.3}_{-0.0}) \cdot 10^{-5}$	$2.0 \cdot 10^{-5}$	3	0.0	0.93
36200.0 – 51200.0	43100	$(5.3\,^{+12.1}_{-4.2}\,^{+1.3}_{-0.2}) \cdot 10^{-6}$	$3.3 \cdot 10^{-6}$	1	0.0	0.93

Table 1: *The differential cross-section $d\sigma/dQ^2$ for the reaction $e^- p \to e^- X$. The following quantities are given for each bin: the Q^2 range, the value at which the cross section is quoted, Q_c^2, the measured cross-section $d\sigma/dQ^2$ corrected to the Born level and the corresponding cross section predicted by the SM using CTEQ5D PDFs. The first error of the measured cross section gives the statistical error and the second is the systematic uncertainty. The last three columns contain the number of observed events in data, N_{obs}, the number of expected background events, N_{bg} and the acceptance, $\mathcal{A}$.*

Q_c^2 (GeV^2)	$d\sigma/dQ^2$ (pb / GeV^2)	stat. (%)	total sys. (%)	uncor. sys. (%)	δ_1 (%)	δ_2 (%)	δ_3 (%)	δ_4 (%)	δ_5 (%)	δ_6 (%)
250	11.150	$^{+0.9}_{-0.9}$	$^{+1.0}_{-1.4}$	$^{+0.8}_{-0.6}$	$^{-0.3}_{+0.4}$	$^{}_{+0.0}$	$^{+0.0}_{+0.0}$	$^{-0.6}_{+0.4}$	$^{+0.2}_{-1.0}$	$^{+0.1}_{-0.3}$
350	5.005	$^{+1.4}_{-1.4}$	$^{+0.7}_{-1.7}$	$^{+0.5}_{-0.8}$	$^{-0.5}_{+0.3}$	$^{}_{-0.2}$	$^{-0.1}_{-0.2}$	$^{-0.8}_{-0.1}$	$^{+0.0}_{-1.1}$	$^{-0.2}_{+0.5}$
440	2.854	$^{+2.1}_{-2.1}$	$^{+0.9}_{-1.7}$	$^{+0.7}_{-0.8}$	$^{-0.3}_{+0.3}$	$^{}_{+0.1}$	$^{+0.1}_{-0.1}$	$^{-0.6}_{+0.0}$	$^{+0.3}_{-1.1}$	$^{+0.4}_{-0.9}$
520	1.876	$^{+2.6}_{-2.5}$	$^{+1.4}_{-1.7}$	$^{+1.0}_{-1.3}$	$^{-0.2}_{+0.4}$	$^{}_{+0.1}$	$^{-0.0}_{+0.1}$	$^{-0.2}_{+0.6}$	$^{+0.3}_{-0.9}$	$^{-0.2}_{+0.5}$
620	1.198	$^{+3.2}_{-3.1}$	$^{+1.1}_{-2.0}$	$^{+1.0}_{-1.2}$	$^{-0.5}_{+0.3}$	$^{}_{-0.2}$	$^{-0.2}_{+0.1}$	$^{-1.0}_{+0.2}$	$^{+0.1}_{-0.8}$	$^{+0.3}_{-0.6}$
730	$8.82 \cdot 10^{-1}$	$^{+3.2}_{-3.1}$	$^{+1.1}_{-1.1}$	$^{+0.8}_{-0.4}$	$^{-0.2}_{+0.4}$	$^{}_{+0.2}$	$^{-0.0}_{+0.1}$	$^{-0.5}_{+0.5}$	$^{+0.3}_{-0.7}$	$^{+0.2}_{-0.4}$
870	$5.27 \cdot 10^{-1}$	$^{+3.2}_{-3.1}$	$^{+1.4}_{-1.8}$	$^{+1.2}_{-0.7}$	$^{+0.1}_{+0.2}$	$^{}_{-0.2}$	$^{+0.1}_{-0.0}$	$^{-0.6}_{-0.2}$	$^{+0.5}_{-1.0}$	$^{+0.5}_{-1.2}$
1040	$3.36 \cdot 10^{-1}$	$^{+3.5}_{-3.4}$	$^{+1.7}_{-1.1}$	$^{+1.1}_{-0.3}$	$^{+0.1}_{+0.2}$	$^{}_{-0.3}$	$^{+0.0}_{-0.0}$	$^{-0.2}_{+1.2}$	$^{+0.3}_{-0.9}$	$^{-0.2}_{+0.5}$
1230	$2.15 \cdot 10^{-1}$	$^{+4.0}_{-3.9}$	$^{+1.8}_{-0.9}$	$^{+1.1}_{-0.4}$	$^{+0.1}_{+0.4}$	$^{}_{-0.4}$	$^{+0.3}_{+0.0}$	$^{-0.3}_{+1.2}$	$^{+0.4}_{-0.6}$	$^{+0.1}_{-0.3}$
1470	$1.54 \cdot 10^{-1}$	$^{+4.3}_{-4.1}$	$^{+1.3}_{-1.7}$	$^{+0.7}_{-0.7}$	$^{-0.2}_{+0.1}$	$^{}_{-0.2}$	$^{+0.1}_{+0.4}$	$^{-1.1}_{+0.6}$	$^{+0.2}_{-1.0}$	$^{-0.3}_{+0.8}$
1740	$9.76 \cdot 10^{-2}$	$^{+4.9}_{-4.7}$	$^{+1.8}_{-1.6}$	$^{+1.3}_{-0.5}$	$^{+0.1}_{+0.3}$	$^{}_{+0.5}$	$^{+0.3}_{+0.2}$	$^{-0.2}_{+0.8}$	$^{+0.5}_{-0.8}$	$^{+0.6}_{-1.3}$
2100	$5.34 \cdot 10^{-2}$	$^{+6.0}_{-5.7}$	$^{+1.6}_{-1.5}$	$^{+1.3}_{-0.3}$	$^{+0.1}_{+0.3}$	$^{}_{+0.1}$	$^{+0.1}_{-0.4}$	$^{+0.5}_{+0.6}$	$^{+0.3}_{-0.7}$	$^{+0.5}_{-1.2}$
2500	$3.82 \cdot 10^{-2}$	$^{+6.5}_{-6.1}$	$^{+2.6}_{-2.0}$	$^{+1.4}_{-0.4}$	$^{+0.3}_{+0.4}$	$^{}_{-0.2}$	$^{+0.1}_{+1.0}$	$^{+0.3}_{+1.7}$	$^{+0.6}_{-0.8}$	$^{+0.7}_{-1.7}$
2900	$2.45 \cdot 10^{-2}$	$^{+7.8}_{-7.3}$	$^{+1.8}_{-1.3}$	$^{+1.3}_{-0.9}$	$^{+0.2}_{+0.3}$	$^{}_{-0.1}$	$^{-0.3}_{+0.8}$	$^{+0.2}_{+0.3}$	$^{+0.4}_{-0.9}$	$^{-0.2}_{+0.6}$
3800	$1.39 \cdot 10^{-2}$	$^{+6.1}_{-5.8}$	$^{+1.9}_{-3.1}$	$^{+1.6}_{-0.8}$	$^{+0.0}_{+0.3}$	$^{}_{-2.1}$	$^{-0.2}_{+0.2}$	$^{-1.4}_{+0.5}$	$^{+0.3}_{-0.9}$	$^{+0.6}_{-1.4}$
5400	$5.05 \cdot 10^{-3}$	$^{+8.7}_{-8.1}$	$^{+2.5}_{-2.3}$	$^{+1.4}_{-0.9}$	$^{+0.2}_{+0.4}$	$^{}_{-0.0}$	$^{+1.3}_{-0.2}$	$^{-1.9}_{+1.4}$	$^{+0.6}_{-0.7}$	$^{+0.2}_{-0.5}$
7600	$2.13 \cdot 10^{-3}$	$^{+12.}_{-11.}$	$^{+1.6}_{-2.1}$	$^{+0.5}_{-1.2}$	$^{-0.3}_{+0.2}$	$^{}_{-1.3}$	$^{+0.6}_{+1.5}$	$^{-0.1}_{-0.2}$	$^{+0.2}_{-1.1}$	$^{+0.2}_{-0.4}$
10800	$6.0 \cdot 10^{-4}$	$^{+20.}_{-17.}$	$^{+4.3}_{-1.6}$	$^{+3.0}_{-0.7}$	$^{-0.5}_{+0.5}$	$^{}_{+1.8}$	$^{-0.7}_{+1.9}$	$^{+1.5}_{-0.3}$	$^{+0.3}_{-1.0}$	$^{+0.2}_{-0.5}$
15200	$3.2 \cdot 10^{-4}$	$^{+24.}_{-20.}$	$^{+7.8}_{-3.0}$	$^{+0.7}_{-0.3}$	$^{-0.6}_{+0.8}$	$^{}_{+5.4}$	$^{-1.1}_{+3.5}$	$^{-2.4}_{+3.8}$	$^{+0.3}_{-0.9}$	$^{-0.8}_{+1.9}$
21500	$7.1 \cdot 10^{-5}$	$^{+50.}_{-35.}$	$^{+5.0}_{-5.1}$	$^{+1.2}_{-0.5}$	$^{-0.5}_{+0.5}$	$^{}_{-4.7}$	$^{-1.2}_{+4.2}$	$^{+2.3}_{-0.6}$	$^{+0.2}_{-1.0}$	$^{+0.3}_{-0.7}$
30400	$2.0 \cdot 10^{-5}$	$^{+97.}_{-53.}$	$^{+13.}_{-2.4}$	$^{+0.8}_{-0.5}$	$^{-0.5}_{+0.8}$	$^{}_{+11.}$	$^{-1.9}_{+5.0}$	$^{+2.8}_{-0.3}$	$^{+0.2}_{-0.9}$	$^{-0.7}_{+1.6}$
43100	$5.3 \cdot 10^{-6}$	$^{+230.}_{-80.}$	$^{+24.}_{-3.9}$	$^{+1.0}_{-1.4}$	$^{-1.1}_{+1.4}$	$^{}_{+23.}$	$^{-2.4}_{+5.5}$	$^{+0.3}_{+0.0}$	$^{+0.2}_{-1.0}$	$^{-2.3}_{+5.3}$

Table 2: *Systematic uncertainties with bin-to-bin correlations for the differential cross-section $d\sigma/dQ^2$. The left part of the table contains the quoted Q^2 value, Q_c^2, the measured cross section $d\sigma/dQ^2$ corrected to the Born level, the statistical error and the total systematic uncertainty. The right part of the table lists the total uncorrelated systematic uncertainty followed by the uncertainties δ_1–δ_6 (see text) with bin-to-bin correlations. For the latter, the upper (lower) numbers refer to positive (negative) variation of e.g. the cut value, whereas the signs of the numbers reflect the direction of change in the cross sections.*

Q^2 cut (GeV^2)	x range	x_c	$d\sigma/dx$ (pb)		N_{obs}	N_{bg}	$\mathcal{A}$
			measured	SM			
200	$(0.63 - 1.00)\cdot 10^{-2}$	$0.794\cdot 10^{-2}$	$(7.91 \pm 0.15\,^{+0.12}_{-0.12})\cdot 10^4$	$8.02\cdot 10^4$	3834	4.3	0.81
	$(0.10 - 0.16)\cdot 10^{-1}$	$0.126\cdot 10^{-1}$	$(5.56 \pm 0.09\,^{+0.13}_{-0.11})\cdot 10^4$	$5.40\cdot 10^4$	4545	3.2	0.83
	$(0.16 - 0.25)\cdot 10^{-1}$	$0.200\cdot 10^{-1}$	$(3.40 \pm 0.06\,^{+0.03}_{-0.04})\cdot 10^4$	$3.38\cdot 10^4$	4396	1.9	0.86
	$(0.25 - 0.40)\cdot 10^{-1}$	$0.316\cdot 10^{-1}$	$(2.02 \pm 0.03\,^{+0.02}_{-0.03})\cdot 10^4$	$2.02\cdot 10^4$	4472	1.7	0.88
	$(0.40 - 0.63)\cdot 10^{-1}$	$0.501\cdot 10^{-1}$	$(1.16 \pm 0.02\,^{+0.02}_{-0.02})\cdot 10^4$	$1.17\cdot 10^4$	3999	1.1	0.89
	$(0.63 - 1.00)\cdot 10^{-1}$	$0.794\cdot 10^{-1}$	$(6.41 \pm 0.12\,^{+0.10}_{-0.19})\cdot 10^3$	$6.65\cdot 10^3$	3724	0.3	0.93
	$0.10 - 0.16$	0.126	$(3.54 \pm 0.07\,^{+0.05}_{-0.08})\cdot 10^3$	$3.66\cdot 10^3$	3468	0.0	0.98
	$0.16 - 0.25$	0.200	$(1.91 \pm 0.05\,^{+0.04}_{-0.04})\cdot 10^3$	$1.89\cdot 10^3$	2218	0.0	0.76
	$0.25 - 0.40$	0.316	$(8.23 \pm 0.39\,^{+0.26}_{-0.25})\cdot 10^2$	$8.15\cdot 10^2$	550	0.0	0.27
10 000	$0.10 - 0.16$	0.126	$4.51\,^{+4.36}_{-2.41}\,^{+0.68}_{-0.28}$	13.20	3	0.0	0.87
	$0.16 - 0.25$	0.200	$(2.05\,^{+0.48}_{-0.40}\,^{+0.12}_{-0.06})\cdot 10^1$	$1.66\cdot 10^1$	26	0.0	0.90
	$0.25 - 0.40$	0.316	$(1.11\,^{+0.27}_{-0.22}\,^{+0.05}_{-0.02})\cdot 10^1$	$0.96\cdot 10^1$	25	0.0	0.92
	$0.40 - 0.63$	0.501	$2.74\,^{+1.14}_{-0.83}\,^{+0.31}_{-0.04}$	2.53	10	0.0	0.93

Table 3: *The differential cross-section $d\sigma/dx$ for the reaction $e^- p \to e^- X$. The following quantities are given for each bin: the lower Q^2 cut, the x range, the value at which the cross section is quoted, x_c, the measured $d\sigma/dx$ corrected to the Born level and the corresponding cross section predicted by the SM using CTEQ5D PDFs. The first error of the measured cross section gives the statistical error and the second is the systematic uncertainty. The last three columns contain the number of observed events in data, N_{obs}, the number of expected background events, N_{bg} and the acceptance, $\mathcal{A}$.*

Q^2 cut (GeV^2)	x_c	$d\sigma/dx$ (pb)	stat. (%)	total sys. (%)	uncor. sys. (%)	δ_1 (%)	δ_2 (%)	δ_3 (%)	δ_4 (%)	δ_5 (%)	δ_6 (%)
200	$0.794 \cdot 10^{-2}$	$7.91 \cdot 10^4$	$^{+1.9}_{-1.8}$	$^{+1.5}_{-1.5}$	$^{+1.3}_{-0.8}$	$^{-0.2}_{+0.4}$	$+0.0$	$^{+0.1}_{-0.1}$	$^{-1.0}_{+0.6}$	$^{+0.2}_{-0.9}$	$^{-0.3}_{+0.8}$
	$0.126 \cdot 10^{-1}$	$5.56 \cdot 10^4$	$^{+1.7}_{-1.7}$	$^{+2.3}_{-2.1}$	$^{+1.1}_{-1.1}$	$^{-0.1}_{+0.1}$	-0.2	$^{-0.0}_{+0.0}$	$^{-1.4}_{+0.7}$	$^{+0.2}_{-1.0}$	$^{-0.8}_{+1.9}$
	$0.200 \cdot 10^{-1}$	$3.40 \cdot 10^4$	$^{+1.7}_{-1.7}$	$^{+1.0}_{-1.1}$	$^{+1.1}_{-0.9}$	$^{-0.0}_{+0.3}$	$+0.1$	$^{+0.1}_{+0.1}$	$^{-0.5}_{+0.2}$	$^{+0.3}_{-0.9}$	$^{+0.1}_{-0.1}$
	$0.316 \cdot 10^{-1}$	$2.02 \cdot 10^4$	$^{+1.7}_{-1.7}$	$^{+0.8}_{-1.7}$	$^{+1.1}_{-1.7}$	$^{-0.1}_{+0.2}$	-0.1	$^{+0.1}_{+0.1}$	$^{-0.5}_{+0.4}$	$^{+0.2}_{-1.0}$	$^{+0.2}_{-0.6}$
	$0.501 \cdot 10^{-1}$	$1.16 \cdot 10^4$	$^{+1.8}_{-1.8}$	$^{+1.4}_{-1.7}$	$^{+1.5}_{-1.3}$	$^{-0.1}_{+0.3}$	-0.0	$^{+0.0}_{+0.1}$	$^{-0.1}_{+0.3}$	$^{+0.3}_{-0.9}$	$^{+0.5}_{-1.2}$
	$0.794 \cdot 10^{-1}$	$6.41 \cdot 10^3$	$^{+1.9}_{-1.8}$	$^{+1.5}_{-2.9}$	$^{+1.3}_{-1.1}$	$^{-0.1}_{+0.3}$	$+0.0$	$^{-0.0}_{-0.0}$	$^{-0.9}_{-0.0}$	$^{+0.3}_{-1.0}$	$^{+1.0}_{-2.4}$
	0.126	$3.54 \cdot 10^3$	$^{+1.9}_{-1.9}$	$^{+1.4}_{-2.1}$	$^{+1.7}_{-0.8}$	$^{-0.1}_{+0.2}$	$+0.1$	$^{-0.0}_{+0.0}$	$^{-0.6}_{-0.4}$	$^{+0.3}_{-0.9}$	$^{+0.7}_{-1.8}$
	0.200	$1.91 \cdot 10^3$	$^{+2.4}_{-2.4}$	$^{+1.9}_{-2.1}$	$^{+2.1}_{-1.2}$	$^{+0.0}_{+0.1}$	$+0.0$	$^{+0.0}_{+0.1}$	$^{-1.1}_{+0.3}$	$^{+0.3}_{-0.9}$	$^{+0.4}_{-0.9}$
	0.316	$8.23 \cdot 10^2$	$^{+4.7}_{-4.5}$	$^{+3.1}_{-3.0}$	$^{+3.1}_{-2.9}$	$^{+0.1}_{+0.5}$	$+0.2$	$^{+0.3}_{+0.3}$	$^{+0.8}_{-0.1}$	$^{+0.4}_{-0.6}$	$^{+0.3}_{-0.7}$
10 000	0.126	4.51	$^{+97.}_{-53.}$	$^{+15.}_{-6.1}$	$^{+4.4}_{-6.5}$	$^{-2.0}_{+2.5}$	$+13.$	$^{-1.4}_{+5.0}$	$^{+3.1}_{-0.4}$	$^{+0.3}_{-1.1}$	$^{+2.3}_{-5.3}$
	0.200	$2.05 \cdot 10^1$	$^{+24.}_{-19.}$	$^{+5.7}_{-2.7}$	$^{+2.9}_{-1.2}$	$^{-0.4}_{+0.5}$	$+2.5$	$^{-1.2}_{+3.5}$	$^{-2.1}_{+3.6}$	$^{+0.3}_{-1.0}$	$^{-0.2}_{+0.6}$
	0.316	$1.11 \cdot 10^1$	$^{+24.}_{-20.}$	$^{+4.2}_{-1.7}$	$^{+1.7}_{-1.4}$	$^{-0.2}_{+0.2}$	$+2.3$	$^{-0.7}_{+2.5}$	$^{+1.6}_{-0.4}$	$^{+0.3}_{-0.9}$	$^{-0.8}_{+1.8}$
	0.501	2.74	$^{+42.}_{-30.}$	$^{+11.}_{-1.5}$	$^{+10.}_{-2.4}$	$^{-0.1}_{+0.9}$	$+1.4$	$^{-0.4}_{+2.0}$	$^{+1.3}_{+0.5}$	$^{+0.3}_{-0.4}$	$^{-1.3}_{+3.2}$

Table 4: *Systematic uncertainties with bin-to-bin correlations for the differential cross-section $d\sigma/dx$. The left part of the table contains the lower Q^2 cut, the quoted x value, x_c, the measured cross-section $d\sigma/dx$ corrected to the Born level, the statistical error and the total systematic uncertainty. The right part of the table lists the total uncorrelated systematic uncertainty followed by the uncertainties δ_1–δ_6 (see text) with bin-to-bin correlations. For the latter, the upper (lower) numbers refer to positive (negative) variation of e.g. the cut value, whereas the signs of the numbers reflect the direction of change in the cross sections.*

Q^2 cut (GeV^2)	y range	y_c	$d\sigma/dy$ (pb)		N_{obs}	N_{bg}	$\mathcal{A}$
			measured	SM			
200	0.05 – 0.10	0.075	$(\,7.44 \pm 0.11\,^{+0.08}_{-0.11}) \cdot 10^3$	$7.50 \cdot 10^3$	5709	0.1	0.89
	0.10 – 0.15	0.125	$(\,5.26 \pm 0.10\,^{+0.03}_{-0.08}) \cdot 10^3$	$5.21 \cdot 10^3$	3879	0.1	0.86
	0.15 – 0.20	0.175	$(\,4.16 \pm 0.09\,^{+0.07}_{-0.06}) \cdot 10^3$	$4.02 \cdot 10^3$	2947	0.2	0.84
	0.20 – 0.25	0.225	$(\,3.31 \pm 0.08\,^{+0.09}_{-0.06}) \cdot 10^3$	$3.28 \cdot 10^3$	2327	0.1	0.83
	0.25 – 0.30	0.275	$(\,2.63 \pm 0.07\,^{+0.03}_{-0.05}) \cdot 10^3$	$2.75 \cdot 10^3$	1850	0.0	0.83
	0.30 – 0.35	0.325	$(\,2.43 \pm 0.07\,^{+0.03}_{-0.06}) \cdot 10^3$	$2.36 \cdot 10^3$	1663	0.6	0.82
	0.35 – 0.40	0.375	$(\,2.09 \pm 0.06\,^{+0.03}_{-0.04}) \cdot 10^3$	$2.06 \cdot 10^3$	1453	0.5	0.84
	0.40 – 0.45	0.425	$(\,1.77 \pm 0.06\,^{+0.02}_{-0.04}) \cdot 10^3$	$1.82 \cdot 10^3$	1212	0.8	0.81
	0.45 – 0.50	0.475	$(\,1.65 \pm 0.06\,^{+0.05}_{-0.02}) \cdot 10^3$	$1.62 \cdot 10^3$	1134	0.9	0.81
	0.50 – 0.55	0.525	$(\,1.40 \pm 0.05\,^{+0.02}_{-0.04}) \cdot 10^3$	$1.45 \cdot 10^3$	933	1.6	0.77
	0.55 – 0.60	0.575	$(\,1.31 \pm 0.05\,^{+0.03}_{-0.02}) \cdot 10^3$	$1.31 \cdot 10^3$	849	1.6	0.76
	0.60 – 0.65	0.625	$(\,1.18 \pm 0.05\,^{+0.04}_{-0.02}) \cdot 10^3$	$1.20 \cdot 10^3$	695	1.3	0.69
	0.65 – 0.70	0.675	$(\,1.16 \pm 0.05\,^{+0.07}_{-0.03}) \cdot 10^3$	$1.10 \cdot 10^3$	637	1.1	0.63
	0.70 – 0.75	0.725	$(\,9.02 \pm 0.48\,^{+0.26}_{-0.57}) \cdot 10^2$	$10.08 \cdot 10^2$	454	1.7	0.59

Table 5: *The differential cross-section $d\sigma/dy$ for the reaction $e^- p \to e^- X$. The following quantities are given for each bin: the lower Q^2 cut, the y range, the value at which the cross section is quoted, y_c, the measured cross-section $d\sigma/dy$ corrected to the Born level and the corresponding cross section predicted by the SM using CTEQ5D fit PDFs. The first error of the measured cross section gives the statistical error and the second is the systematic uncertainty. The last three columns contain the number of observed events in data, N_{obs}, the number of expected background events, N_{bg} and the acceptance, $\mathcal{A}$.*

Q^2 cut (GeV^2)	y_c	$d\sigma/dy$ (pb)	stat. (%)	total sys. (%)	uncor. sys. (%)	δ_1 (%)	δ_2 (%)	δ_3 (%)	δ_4 (%)	δ_5 (%)	δ_6 (%)
200	0.075	$7.44 \cdot 10^3$	$^{+1.5}_{-1.5}$	$^{+1.0}_{-1.5}$	$^{+4.4}_{-6.5}$	$^{-0.1}_{+0.3}$	$+0.0$	$^{-0.0}_{+0.1}$	$^{-0.2}_{+0.4}$	$^{+0.3}_{-0.9}$	$^{+0.4}_{-1.0}$
	0.125	$5.26 \cdot 10^3$	$^{+1.8}_{-1.8}$	$^{+0.5}_{-1.6}$	$^{+3.0}_{-1.5}$	$^{-0.1}_{+0.1}$	-0.0	$^{+0.0}_{-0.0}$	$^{-0.9}_{-0.1}$	$^{+0.2}_{-1.0}$	$^{+0.2}_{-0.5}$
	0.175	$4.16 \cdot 10^3$	$^{+2.1}_{-2.1}$	$^{+1.8}_{-1.4}$	$^{+1.9}_{-1.5}$	$^{-0.2}_{+0.2}$	$+0.1$	$^{+0.1}_{+0.1}$	$^{-0.7}_{+0.1}$	$^{+0.2}_{-0.9}$	$^{-0.6}_{+1.5}$
	0.225	$3.31 \cdot 10^3$	$^{+2.4}_{-2.3}$	$^{+2.7}_{-1.7}$	$^{+10.}_{-2.5}$	$^{+0.0}_{+0.2}$	$+0.1$	$^{+0.0}_{+0.1}$	$^{-0.6}_{+0.5}$	$^{+0.3}_{-0.9}$	$^{-1.0}_{+2.4}$
	0.275	$2.63 \cdot 10^3$	$^{+2.6}_{-2.6}$	$^{+1.3}_{-1.8}$	$^{+2.7}_{-2.0}$	$^{-0.2}_{+0.0}$	-0.2	$^{-0.1}_{+0.0}$	$^{-0.4}_{+0.3}$	$^{+0.2}_{-1.1}$	$^{-0.1}_{+0.2}$
	0.325	$2.43 \cdot 10^3$	$^{+2.8}_{-2.8}$	$^{+1.1}_{-2.4}$	$^{+1.9}_{-2.0}$	$^{-0.3}_{+0.0}$	-0.2	$^{-0.1}_{-0.2}$	$^{-1.8}_{+0.6}$	$^{+0.1}_{-1.1}$	$^{+0.0}_{+0.1}$
	0.375	$2.09 \cdot 10^3$	$^{+3.0}_{-2.9}$	$^{+1.5}_{-1.9}$	$^{+3.1}_{-5.6}$	$^{-0.2}_{+0.2}$	-0.1	$^{+0.0}_{-0.2}$	$^{-1.5}_{+0.4}$	$^{+0.1}_{-0.9}$	$^{-0.4}_{+1.1}$
	0.425	$1.77 \cdot 10^3$	$^{+3.3}_{-3.2}$	$^{+0.9}_{-2.0}$	$^{+2.5}_{-2.0}$	$^{-0.2}_{+0.1}$	-0.0	$^{-0.1}_{-0.2}$	$^{-0.9}_{-0.1}$	$^{+0.1}_{-1.1}$	$^{-0.1}_{+0.3}$
	0.475	$1.65 \cdot 10^3$	$^{+3.4}_{-3.3}$	$^{+2.8}_{-1.5}$	$^{+3.8}_{-2.9}$	$^{+0.0}_{+0.3}$	$+0.1$	$^{-0.1}_{+0.2}$	$^{-0.9}_{+0.7}$	$^{+0.5}_{-0.9}$	$^{-0.6}_{+1.4}$
	0.525	$1.40 \cdot 10^3$	$^{+3.7}_{-3.6}$	$^{+1.4}_{-2.8}$	$^{+1.0}_{-2.3}$	$^{-0.3}_{+0.4}$	-0.3	$^{+0.1}_{-0.1}$	$^{-1.0}_{+0.6}$	$^{+0.3}_{-1.1}$	$^{-0.5}_{+1.0}$
	0.575	$1.31 \cdot 10^3$	$^{+3.9}_{-3.8}$	$^{+2.5}_{-1.5}$	$^{+2.4}_{-0.6}$	$^{-0.3}_{+0.7}$	$+0.3$	$^{+0.2}_{-0.0}$	$^{+0.5}_{+1.1}$	$^{+0.6}_{-1.0}$	$^{+0.5}_{-1.0}$
	0.625	$1.18 \cdot 10^3$	$^{+4.3}_{-4.2}$	$^{+3.3}_{-2.1}$	$^{+2.4}_{-1.5}$	$^{-1.2}_{+1.2}$	$+0.2$	$^{-0.2}_{+0.5}$	$^{+2.1}_{+0.8}$	$^{+0.4}_{-0.9}$	$^{-0.3}_{+0.8}$
	0.675	$1.16 \cdot 10^3$	$^{+4.5}_{-4.4}$	$^{+5.6}_{-2.2}$	$^{+4.1}_{-1.0}$	$^{-1.3}_{+2.3}$	$+0.4$	$^{-0.1}_{+0.8}$	$^{-1.0}_{+2.1}$	$^{+0.2}_{-0.6}$	$^{-1.1}_{+2.5}$
	0.725	$9.02 \cdot 10^2$	$^{+5.3}_{-5.1}$	$^{+2.8}_{-6.3}$	$^{+1.7}_{-5.1}$	$^{-3.1}_{+1.3}$	-0.9	$^{+0.0}_{-0.8}$	$^{-0.3}_{+2.0}$	$^{-1.1}_{-1.7}$	$^{-0.5}_{+1.2}$

Table 6: *Systematic uncertainties with bin-to-bin correlations for the differential cross-section $d\sigma/dy$. The left part of the table contains the lower Q^2 cut, the quoted y value, y_c, the measured cross-section $d\sigma/dy$ corrected to the Born level, the statistical error and the total systematic uncertainty. The right part of the table lists the total uncorrelated systematic uncertainty followed by the uncertainties δ_1–δ_6 (see text) with bin-to-bin correlations. For the latter, the upper (lower) numbers refer to positive (negative) variation of e.g. the cut value, whereas the signs of the numbers reflect the direction of change in the cross sections.*

Q^2 range (GeV^2)	x range	Q_c^2 (GeV^2)	x_c	$\tilde{\sigma}(e^-p)$		N_{obs}	N_{bg}	$\mathcal{A}$
				measured	SM			
185. – 240.	$(0.37 - 0.60) \cdot 10^{-2}$	200	$0.50 \cdot 10^{-2}$	$1.137 \pm 0.032\,^{+0.034}_{-0.024}$	1.106	1743	1.0	0.89
	$(0.60 - 1.00) \cdot 10^{-2}$		$0.80 \cdot 10^{-2}$	$(9.52 \pm 0.26\,^{+0.20}_{-0.15}) \cdot 10^{-1}$	$9.44 \cdot 10^{-1}$	1823	0.1	0.91
	$(0.10 - 0.17) \cdot 10^{-1}$		$0.13 \cdot 10^{-1}$	$(8.16 \pm 0.23\,^{+0.19}_{-0.15}) \cdot 10^{-1}$	$8.00 \cdot 10^{-1}$	1791	0.0	0.90
	$(0.17 - 0.25) \cdot 10^{-1}$		$0.21 \cdot 10^{-1}$	$(7.05 \pm 0.24\,^{+0.14}_{-0.10}) \cdot 10^{-1}$	$6.79 \cdot 10^{-1}$	1238	0.1	0.92
	$(0.25 - 0.37) \cdot 10^{-1}$		$0.32 \cdot 10^{-1}$	$(5.90 \pm 0.21\,^{+0.06}_{-0.12}) \cdot 10^{-1}$	$5.90 \cdot 10^{-1}$	1143	0.0	0.96
	$(0.37 - 0.60) \cdot 10^{-1}$		$0.50 \cdot 10^{-1}$	$(5.02 \pm 0.17\,^{+0.09}_{-0.12}) \cdot 10^{-1}$	$5.13 \cdot 10^{-1}$	1277	0.2	0.98
	$(0.60 - 1.20) \cdot 10^{-1}$		$0.80 \cdot 10^{-1}$	$(4.23 \pm 0.12\,^{+0.09}_{-0.15}) \cdot 10^{-1}$	$4.42 \cdot 10^{-1}$	1659	0.0	1.09
	0.12 – 0.25		0.18	$(3.22 \pm 0.12\,^{+0.04}_{-0.13}) \cdot 10^{-1}$	$3.28 \cdot 10^{-1}$	948	0.0	0.75
240. – 310.	$(0.37 - 0.60) \cdot 10^{-2}$	250	$0.50 \cdot 10^{-2}$	$1.08 \pm 0.05\,^{+0.04}_{-0.04}$	1.13	751	0.7	0.58
	$(0.60 - 1.00) \cdot 10^{-2}$		$0.80 \cdot 10^{-2}$	$(9.75 \pm 0.31\,^{+0.19}_{-0.23}) \cdot 10^{-1}$	$9.64 \cdot 10^{-1}$	1327	0.6	0.90
	$(0.10 - 0.17) \cdot 10^{-1}$		$0.13 \cdot 10^{-1}$	$(8.61 \pm 0.28\,^{+0.19}_{-0.18}) \cdot 10^{-1}$	$8.16 \cdot 10^{-1}$	1354	0.1	0.89
	$(0.17 - 0.25) \cdot 10^{-1}$		$0.21 \cdot 10^{-1}$	$(6.94 \pm 0.27\,^{+0.06}_{-0.13}) \cdot 10^{-1}$	$6.90 \cdot 10^{-1}$	905	0.0	0.91
	$(0.25 - 0.37) \cdot 10^{-1}$		$0.32 \cdot 10^{-1}$	$(6.11 \pm 0.25\,^{+0.08}_{-0.20}) \cdot 10^{-1}$	$5.97 \cdot 10^{-1}$	877	0.0	0.95
	$(0.37 - 0.60) \cdot 10^{-1}$		$0.50 \cdot 10^{-1}$	$(5.24 \pm 0.20\,^{+0.09}_{-0.14}) \cdot 10^{-1}$	$5.17 \cdot 10^{-1}$	960	0.1	0.95
	$(0.60 - 1.20) \cdot 10^{-1}$		$0.80 \cdot 10^{-1}$	$(4.36 \pm 0.15\,^{+0.07}_{-0.22}) \cdot 10^{-1}$	$4.44 \cdot 10^{-1}$	1204	0.0	1.00
	0.12 – 0.25		0.18	$(2.98 \pm 0.12\,^{+0.20}_{-0.08}) \cdot 10^{-1}$	$3.26 \cdot 10^{-1}$	817	0.0	0.90

Table 7: *The reduced cross-section $\tilde{\sigma}(e^-p)$ for the reaction $e^-p \to e^-X$. The following quantities are given for each bin: the Q^2 and x ranges, the values at which the cross section is quoted, Q_c^2 and x_c, the measured reduced cross-section, $\tilde{\sigma}(e^-p)$, corrected to Born level and the corresponding cross section predicted by the SM using CTEQ5D PDFs. The first error of the measured cross section gives the statistical error and the second is the systematic uncertainty. The last three columns contain the number of observed events in data, N_{obs}, the number of expected background events, N_{bg} and the acceptance, $\mathcal{A}$.*

Q^2 range (GeV^2)	x range	Q_c^2 (GeV^2)	x_c	$\tilde{\sigma}(e^-p)$		N_{obs}	N_{bg}	$\mathcal{A}$
				measured	SM			
310. – 410.	$(0.60 - 1.00) \cdot 10^{-2}$	350	$0.80 \cdot 10^{-2}$	$(9.80 \pm 0.45\,^{+0.17}_{-0.17}) \cdot 10^{-1}$	$9.91 \cdot 10^{-1}$	668	1.3	0.59
	$(0.10 - 0.17) \cdot 10^{-1}$		$0.13 \cdot 10^{-1}$	$(8.51 \pm 0.32\,^{+0.27}_{-0.19}) \cdot 10^{-1}$	$8.39 \cdot 10^{-1}$	980	0.1	0.84
	$(0.17 - 0.25) \cdot 10^{-1}$		$0.21 \cdot 10^{-1}$	$(7.23 \pm 0.31\,^{+0.06}_{-0.19}) \cdot 10^{-1}$	$7.06 \cdot 10^{-1}$	745	0.0	0.91
	$(0.25 - 0.37) \cdot 10^{-1}$		$0.32 \cdot 10^{-1}$	$(5.86 \pm 0.27\,^{+0.05}_{-0.13}) \cdot 10^{-1}$	$6.08 \cdot 10^{-1}$	675	0.0	0.93
	$(0.37 - 0.60) \cdot 10^{-1}$		$0.50 \cdot 10^{-1}$	$(5.27 \pm 0.22\,^{+0.11}_{-0.06}) \cdot 10^{-1}$	$5.23 \cdot 10^{-1}$	776	0.0	0.93
	$(0.60 - 1.20) \cdot 10^{-1}$		$0.80 \cdot 10^{-1}$	$(4.41 \pm 0.17\,^{+0.05}_{-0.10}) \cdot 10^{-1}$	$4.46 \cdot 10^{-1}$	997	0.3	1.01
	$0.12 - 0.25$		0.18	$(3.10 \pm 0.13\,^{+0.09}_{-0.08}) \cdot 10^{-1}$	$3.23 \cdot 10^{-1}$	782	0.0	0.98
410. – 530.	$(0.60 - 1.00) \cdot 10^{-2}$	450	$0.80 \cdot 10^{-2}$	$(9.82 \pm 0.46\,^{+0.21}_{-0.32}) \cdot 10^{-1}$	$10.03 \cdot 10^{-1}$	588	1.5	0.81
	$(0.10 - 0.17) \cdot 10^{-1}$		$0.13 \cdot 10^{-1}$	$(8.37 \pm 0.52\,^{+0.37}_{-0.36}) \cdot 10^{-1}$	$8.55 \cdot 10^{-1}$	332	0.1	0.45
	$(0.17 - 0.25) \cdot 10^{-1}$		$0.21 \cdot 10^{-1}$	$(6.83 \pm 0.41\,^{+0.19}_{-0.09}) \cdot 10^{-1}$	$7.18 \cdot 10^{-1}$	348	0.0	0.67
	$(0.25 - 0.37) \cdot 10^{-1}$		$0.32 \cdot 10^{-1}$	$(6.28 \pm 0.35\,^{+0.12}_{-0.13}) \cdot 10^{-1}$	$6.17 \cdot 10^{-1}$	422	0.0	0.81
	$(0.37 - 0.60) \cdot 10^{-1}$		$0.50 \cdot 10^{-1}$	$(5.08 \pm 0.25\,^{+0.09}_{-0.15}) \cdot 10^{-1}$	$5.28 \cdot 10^{-1}$	519	0.0	0.92
	$(0.60 - 1.00) \cdot 10^{-1}$		$0.80 \cdot 10^{-1}$	$(4.40 \pm 0.22\,^{+0.08}_{-0.08}) \cdot 10^{-1}$	$4.48 \cdot 10^{-1}$	500	0.0	0.96
	$0.10 - 0.17$		0.13	$(3.90 \pm 0.21\,^{+0.06}_{-0.07}) \cdot 10^{-1}$	$3.73 \cdot 10^{-1}$	458	0.0	0.94
	$0.17 - 0.30$		0.25	$(2.83 \pm 0.17\,^{+0.06}_{-0.16}) \cdot 10^{-1}$	$2.59 \cdot 10^{-1}$	365	0.0	0.87

Table 8: *The reduced cross-section $\tilde{\sigma}(e^-p)$ for the reaction $e^-p \to e^-X$. The following quantities are given for each bin: the Q^2 and x ranges, the values at which the cross section is quoted, Q_c^2 and x_c, the measured reduced cross-section, $\tilde{\sigma}(e^-p)$, corrected to Born level and the corresponding cross section predicted by the SM using CTEQ5D PDFs. The first error of the measured cross section gives the statistical error and the second is the systematic uncertainty. The last three columns contain the number of observed events in data, N_{obs}, the number of expected background events, N_{bg} and the acceptance, $\mathcal{A}$.*

Q^2 range (GeV^2)	x range	Q_c^2 (GeV^2)	x_c	$\tilde{\sigma}(e^-p)$		N_{obs}	N_{bg}	$\mathcal{A}$
				measured	SM			
530. – 710.	$(0.60 - 1.00)\cdot 10^{-2}$	650	$0.80\cdot 10^{-2}$	$(9.01 \pm 0.56\,^{+0.23}_{-0.23})\cdot 10^{-1}$	$10.00\cdot 10^{-1}$	328	0.8	0.72
	$(0.10 - 0.17)\cdot 10^{-1}$		$0.13\cdot 10^{-1}$	$(9.19 \pm 0.42\,^{+0.12}_{-0.28})\cdot 10^{-1}$	$8.74\cdot 10^{-1}$	593	0.6	0.87
	$(0.17 - 0.25)\cdot 10^{-1}$		$0.21\cdot 10^{-1}$	$(7.87\,^{+0.53}_{-0.50}\,\,^{+0.09}_{-0.18})\cdot 10^{-1}$	$7.36\cdot 10^{-1}$	289	0.0	0.58
	$(0.25 - 0.37)\cdot 10^{-1}$		$0.32\cdot 10^{-1}$	$(6.01\,^{+0.52}_{-0.48}\,\,^{+0.22}_{-0.07})\cdot 10^{-1}$	$6.29\cdot 10^{-1}$	177	0.0	0.42
	$(0.37 - 0.60)\cdot 10^{-1}$		$0.50\cdot 10^{-1}$	$(5.05\,^{+0.42}_{-0.40}\,\,^{+0.14}_{-0.18})\cdot 10^{-1}$	$5.35\cdot 10^{-1}$	186	0.0	0.41
	$(0.60 - 1.00)\cdot 10^{-1}$		$0.80\cdot 10^{-1}$	$(4.03\,^{+0.35}_{-0.32}\,\,^{+0.08}_{-0.10})\cdot 10^{-1}$	$4.51\cdot 10^{-1}$	177	0.0	0.45
	0.10 – 0.17		0.13	$(3.45\,^{+0.28}_{-0.27}\,\,^{+0.06}_{-0.12})\cdot 10^{-1}$	$3.73\cdot 10^{-1}$	196	0.0	0.51
	0.17 – 0.30		0.25	$(2.63\,^{+0.22}_{-0.21}\,\,^{+0.15}_{-0.10})\cdot 10^{-1}$	$2.55\cdot 10^{-1}$	193	0.0	0.58
710. – 900.	$(0.90 - 1.70)\cdot 10^{-2}$	800	$1.30\cdot 10^{-2}$	$(8.58 \pm 0.48\,^{+0.28}_{-0.10})\cdot 10^{-1}$	$8.81\cdot 10^{-1}$	406	0.8	0.95
	$(0.17 - 0.25)\cdot 10^{-1}$		$0.21\cdot 10^{-1}$	$(8.02\,^{+0.55}_{-0.52}\,\,^{+0.14}_{-0.20})\cdot 10^{-1}$	$7.45\cdot 10^{-1}$	272	0.0	0.97
	$(0.25 - 0.37)\cdot 10^{-1}$		$0.32\cdot 10^{-1}$	$(6.28\,^{+0.46}_{-0.43}\,\,^{+0.12}_{-0.27})\cdot 10^{-1}$	$6.37\cdot 10^{-1}$	241	0.0	0.92
	$(0.37 - 0.60)\cdot 10^{-1}$		$0.50\cdot 10^{-1}$	$(5.84\,^{+0.41}_{-0.39}\,\,^{+0.09}_{-0.14})\cdot 10^{-1}$	$5.40\cdot 10^{-1}$	266	0.0	0.80
	$(0.60 - 1.00)\cdot 10^{-1}$		$0.80\cdot 10^{-1}$	$(4.93\,^{+0.40}_{-0.37}\,\,^{+0.07}_{-0.19})\cdot 10^{-1}$	$4.53\cdot 10^{-1}$	206	0.0	0.70
	0.10 – 0.17		0.13	$(3.43\,^{+0.33}_{-0.31}\,\,^{+0.11}_{-0.23})\cdot 10^{-1}$	$3.73\cdot 10^{-1}$	143	0.0	0.61
	0.17 – 0.30		0.25	$(2.64\,^{+0.31}_{-0.29}\,\,^{+0.18}_{-0.05})\cdot 10^{-1}$	$2.53\cdot 10^{-1}$	99	0.0	0.52

Table 9: *The reduced cross-section $\tilde{\sigma}(e^-p)$ for the reaction $e^-p \to e^-X$. The following quantities are given for each bin: the Q^2 and x ranges, the values at which the cross section is quoted, Q_c^2 and x_c, the measured reduced cross-section, $\tilde{\sigma}(e^-p)$, corrected to Born level and the corresponding cross section predicted by the SM using CTEQ5D PDFs. The first error of the measured cross section gives the statistical error and the second is the systematic uncertainty. The last three columns contain the number of observed events in data, N_{obs}, the number of expected background events, N_{bg} and the acceptance, $\mathcal{A}$.*

Q^2 range (GeV^2)	x range	Q_c^2 (GeV^2)	x_c	$\tilde{\sigma}(e^-p)$		N_{obs}	N_{bg}	$\mathcal{A}$
				measured	SM			
900. – 1300.	$(0.10 - 0.17) \cdot 10^{-1}$	1200	$0.14 \cdot 10^{-1}$	$(8.73\,^{+0.58\ +0.61}_{-0.55\ -0.24}) \cdot 10^{-1}$	$8.61 \cdot 10^{-1}$	284	1.3	0.94
	$(0.17 - 0.25) \cdot 10^{-1}$		$0.21 \cdot 10^{-1}$	$(6.72\,^{+0.49\ +0.12}_{-0.46\ -0.11}) \cdot 10^{-1}$	$7.64 \cdot 10^{-1}$	239	0.2	0.97
	$(0.25 - 0.37) \cdot 10^{-1}$		$0.32 \cdot 10^{-1}$	$(5.82\,^{+0.42\ +0.06}_{-0.40\ -0.18}) \cdot 10^{-1}$	$6.54 \cdot 10^{-1}$	242	0.0	0.97
	$(0.37 - 0.60) \cdot 10^{-1}$		$0.50 \cdot 10^{-1}$	$(5.14\,^{+0.33\ +0.12}_{-0.31\ -0.05}) \cdot 10^{-1}$	$5.52 \cdot 10^{-1}$	311	0.2	0.98
	$(0.60 - 1.00) \cdot 10^{-1}$		$0.80 \cdot 10^{-1}$	$(4.27\,^{+0.28\ +0.07}_{-0.27\ -0.10}) \cdot 10^{-1}$	$4.59 \cdot 10^{-1}$	291	0.0	0.98
	0.10 – 0.17		0.13	$(3.62\,^{+0.25\ +0.12}_{-0.24\ -0.05}) \cdot 10^{-1}$	$3.75 \cdot 10^{-1}$	264	0.0	0.97
	0.17 – 0.30		0.25	$(2.65\,^{+0.21\ +0.04}_{-0.19\ -0.06}) \cdot 10^{-1}$	$2.50 \cdot 10^{-1}$	217	0.0	0.93
	0.30 – 0.53		0.40	$(1.01\,^{+0.15\ +0.04}_{-0.14\ -0.18}) \cdot 10^{-1}$	$1.31 \cdot 10^{-1}$	61	0.0	0.66
1300. – 1800.	$(0.17 - 0.25) \cdot 10^{-1}$	1500	$0.21 \cdot 10^{-1}$	$(7.93\,^{+0.72\ +0.32}_{-0.67\ -0.17}) \cdot 10^{-1}$	$7.72 \cdot 10^{-1}$	152	0.5	1.00
	$(0.25 - 0.37) \cdot 10^{-1}$		$0.32 \cdot 10^{-1}$	$(7.39\,^{+0.63\ +0.18}_{-0.59\ -0.12}) \cdot 10^{-1}$	$6.66 \cdot 10^{-1}$	173	0.4	0.97
	$(0.37 - 0.60) \cdot 10^{-1}$		$0.50 \cdot 10^{-1}$	$(6.03\,^{+0.46\ +0.05}_{-0.43\ -0.15}) \cdot 10^{-1}$	$5.61 \cdot 10^{-1}$	210	0.0	1.00
	$(0.60 - 1.00) \cdot 10^{-1}$		$0.80 \cdot 10^{-1}$	$(4.45\,^{+0.37\ +0.05}_{-0.35\ -0.12}) \cdot 10^{-1}$	$4.65 \cdot 10^{-1}$	176	0.0	0.96
	0.10 – 0.15		0.13	$(3.97\,^{+0.39\ +0.12}_{-0.36\ -0.11}) \cdot 10^{-1}$	$3.77 \cdot 10^{-1}$	131	0.0	0.98
	0.15 – 0.23		0.18	$(3.33\,^{+0.34\ +0.10}_{-0.31\ -0.04}) \cdot 10^{-1}$	$3.18 \cdot 10^{-1}$	124	0.0	1.01
	0.23 – 0.35		0.25	$(2.66\,^{+0.33\ +0.07}_{-0.30\ -0.02}) \cdot 10^{-1}$	$2.50 \cdot 10^{-1}$	84	0.0	0.94
	0.35 – 0.53		0.40	$(1.40\,^{+0.27\ +0.53}_{-0.24\ -0.13}) \cdot 10^{-1}$	$1.30 \cdot 10^{-1}$	38	0.0	0.89

Table 10: *The reduced cross-section $\tilde{\sigma}(e^-p)$ for the reaction $e^-p \to e^-X$. The following quantities are given for each bin: the Q^2 and x ranges, the values at which the cross section is quoted, Q_c^2 and x_c, the measured reduced cross-section, $\tilde{\sigma}(e^-p)$, corrected to Born level and the corresponding cross section predicted by the SM using CTEQ5D PDFs. The first error of the measured cross section gives the statistical error and the second is the systematic uncertainty. The last three columns contain the number of observed events in data, N_{obs}, the number of expected background events, N_{bg} and the acceptance, $\mathcal{A}$.*

Q^2 range (GeV^2)	x range	Q_c^2 (GeV^2)	x_c	$\tilde{\sigma}(e^-p)$		N_{obs}	N_{bg}	$\mathcal{A}$
				measured	SM			
1800. – 2500.	$(0.23 - 0.37) \cdot 10^{-1}$	2000	$0.32 \cdot 10^{-1}$	$(6.93\,^{+0.70\,+0.44}_{-0.65\,-0.11}) \cdot 10^{-1}$	$6.83 \cdot 10^{-1}$	123	1.2	0.98
	$(0.37 - 0.60) \cdot 10^{-1}$		$0.50 \cdot 10^{-1}$	$(5.40\,^{+0.54\,+0.10}_{-0.50\,-0.17}) \cdot 10^{-1}$	$5.77 \cdot 10^{-1}$	123	0.1	0.97
	$(0.60 - 1.00) \cdot 10^{-1}$		$0.80 \cdot 10^{-1}$	$(4.30\,^{+0.44\,+0.11}_{-0.40\,-0.20}) \cdot 10^{-1}$	$4.75 \cdot 10^{-1}$	122	0.0	0.99
	0.10 – 0.15		0.13	$(3.77\,^{+0.45\,+0.16}_{-0.41\,-0.07}) \cdot 10^{-1}$	$3.82 \cdot 10^{-1}$	90	0.0	0.96
	0.15 – 0.23		0.18	$(2.82\,^{+0.37\,+0.09}_{-0.33\,-0.08}) \cdot 10^{-1}$	$3.21 \cdot 10^{-1}$	76	0.0	0.99
	0.23 – 0.35		0.25	$(2.92\,^{+0.42\,+0.07}_{-0.38\,-0.09}) \cdot 10^{-1}$	$2.50 \cdot 10^{-1}$	65	0.0	0.96
	0.35 – 0.53		0.40	$(1.03\,^{+0.25\,+0.10}_{-0.20\,-0.08}) \cdot 10^{-1}$	$1.28 \cdot 10^{-1}$	26	0.0	1.00
2500. – 3500.	$(0.37 - 0.60) \cdot 10^{-1}$	3000	$0.50 \cdot 10^{-1}$	$(6.64\,^{+0.77\,+0.20}_{-0.70\,-0.28}) \cdot 10^{-1}$	$6.11 \cdot 10^{-1}$	95	0.0	0.99
	$(0.60 - 1.00) \cdot 10^{-1}$		$0.80 \cdot 10^{-1}$	$(4.48\,^{+0.55\,+0.11}_{-0.50\,-0.14}) \cdot 10^{-1}$	$5.01 \cdot 10^{-1}$	84	0.0	0.99
	0.10 – 0.15		0.13	$(3.75\,^{+0.55\,+0.11}_{-0.48\,-0.27}) \cdot 10^{-1}$	$3.97 \cdot 10^{-1}$	62	0.0	0.96
	0.15 – 0.23		0.18	$(2.99\,^{+0.47\,+0.10}_{-0.41\,-0.07}) \cdot 10^{-1}$	$3.29 \cdot 10^{-1}$	54	0.0	0.98
	0.23 – 0.35		0.25	$(2.85\,^{+0.50\,+0.13}_{-0.43\,-0.13}) \cdot 10^{-1}$	$2.54 \cdot 10^{-1}$	45	0.0	0.92
	0.35 – 0.53		0.40	$(1.63\,^{+0.41\,+0.10}_{-0.34\,-0.11}) \cdot 10^{-1}$	$1.28 \cdot 10^{-1}$	24	0.0	0.93
	0.53 – 0.75		0.65	$(1.90\,^{+0.96\,+0.18}_{-0.68\,-0.11}) \cdot 10^{-2}$	$1.94 \cdot 10^{-2}$	8	0.0	0.95

Table 11: *The reduced cross-section $\tilde{\sigma}(e^-p)$ for the reaction $e^-p \to e^-X$. The following quantities are given for each bin: the Q^2 and x ranges, the values at which the cross section is quoted, Q_c^2 and x_c, the measured reduced cross-section, $\tilde{\sigma}(e^-p)$, corrected to Born level and the corresponding cross section predicted by the SM using CTEQ5D PDFs. The first error of the measured cross section gives the statistical error and the second is the systematic uncertainty. The last three columns contain the number of observed events in data, N_{obs}, the number of expected background events, N_{bg} and the acceptance, $\mathcal{A}$.*

Q^2 range (GeV^2)	x range	Q_c^2 (GeV^2)	x_c	$\tilde{\sigma}(e^-p)$		N_{obs}	N_{bg}	$\mathcal{A}$
				measured	SM			
3500. – 5600.	$(0.40 - 1.00) \cdot 10^{-1}$	5000	$0.80 \cdot 10^{-1}$	$(5.91\,^{+0.58}_{-0.54}\,^{+0.20}_{-0.07}) \cdot 10^{-1}$	$5.62 \cdot 10^{-1}$	126	0.6	0.96
	0.10 – 0.15		0.13	$(4.39\,^{+0.64}_{-0.56}\,^{+0.12}_{-0.08}) \cdot 10^{-1}$	$4.37 \cdot 10^{-1}$	62	0.0	0.98
	0.15 – 0.23		0.18	$(4.14\,^{+0.59}_{-0.52}\,^{+0.13}_{-0.14}) \cdot 10^{-1}$	$3.55 \cdot 10^{-1}$	65	0.0	0.95
	0.23 – 0.35		0.25	$(2.66\,^{+0.49}_{-0.42}\,^{+0.05}_{-0.08}) \cdot 10^{-1}$	$2.68 \cdot 10^{-1}$	41	0.0	1.02
	0.35 – 0.53		0.40	$(1.60\,^{+0.40}_{-0.33}\,^{+0.06}_{-0.17}) \cdot 10^{-1}$	$1.31 \cdot 10^{-1}$	24	0.0	0.99
5600. – 9000.	$(0.70 - 1.50) \cdot 10^{-1}$	8000	$1.30 \cdot 10^{-1}$	$(5.26\,^{+0.77}_{-0.68}\,^{+0.16}_{-0.26}) \cdot 10^{-1}$	$5.08 \cdot 10^{-1}$	60	0.0	0.91
	0.15 – 0.23		0.18	$(3.82\,^{+0.77}_{-0.65}\,^{+0.13}_{-0.16}) \cdot 10^{-1}$	$4.04 \cdot 10^{-1}$	34	0.0	0.97
	0.23 – 0.35		0.25	$(3.10\,^{+0.73}_{-0.60}\,^{+0.06}_{-0.05}) \cdot 10^{-1}$	$2.97 \cdot 10^{-1}$	26	0.0	1.02
	0.35 – 0.53		0.40	$(1.39\,^{+0.52}_{-0.39}\,^{+0.08}_{-0.11}) \cdot 10^{-1}$	$1.39 \cdot 10^{-1}$	12	0.0	1.00
	0.53 – 0.75		0.65	$(1.9\,^{+1.5}_{-0.9}\,^{+0.1}_{-0.0}) \cdot 10^{-2}$	$1.9 \cdot 10^{-2}$	4	0.0	0.94
9000. – 15000.	0.11 – 0.23	12000	0.18	$(4.5\,^{+1.0}_{-0.8}\,^{+0.3}_{-0.1}) \cdot 10^{-1}$	$4.7 \cdot 10^{-1}$	29	0.0	0.90
	0.23 – 0.35		0.25	$(2.7\,^{+1.0}_{-0.8}\,^{+0.1}_{-0.2}) \cdot 10^{-1}$	$3.4 \cdot 10^{-1}$	12	0.0	0.94
	0.35 – 0.53		0.40	$(1.1\,^{+0.7}_{-0.5}\,^{+0.2}_{-0.0}) \cdot 10^{-1}$	$1.5 \cdot 10^{-1}$	6	0.0	0.99
15000. – 25000.	0.18 – 0.35	20000	0.25	$(4.3\,^{+1.5}_{-1.1}\,^{+0.2}_{-0.1}) \cdot 10^{-1}$	$4.2 \cdot 10^{-1}$	13	0.0	0.92
	0.35 – 0.75		0.40	$(2.1\,^{+1.2}_{-0.8}\,^{+0.1}_{-0.0}) \cdot 10^{-1}$	$1.8 \cdot 10^{-1}$	6	0.0	0.90
25000. – 50000.	0.30 – 0.75	30000	0.40	$(2.3\,^{+1.8}_{-1.1}\,^{+0.3}_{-0.1}) \cdot 10^{-1}$	$2.1 \cdot 10^{-1}$	4	0.0	0.92

Table 12: *The reduced cross-section $\tilde{\sigma}(e^-p)$ for the reaction $e^-p \to e^-X$. The following quantities are given for each bin: the Q^2 and x ranges, the values at which the cross section is quoted, Q_c^2 and x_c, the measured reduced cross-section, $\tilde{\sigma}(e^-p)$, corrected to Born level and the corresponding cross section predicted by the SM using CTEQ5D PDFs. The first error of the measured cross section gives the statistical error and the second is the systematic uncertainty. The last three columns contain the number of observed events in data, N_{obs}, the number of expected background events, N_{bg} and the acceptance, $\mathcal{A}$.*

Q_c^2 (GeV^2)	x_c	$\tilde{\sigma}(e^-p)$	stat. (%)	total sys. (%)	uncor. sys. (%)	δ_1 (%)	δ_2 (%)	δ_3 (%)	δ_4 (%)	δ_5 (%)	δ_6 (%)
200	$0.50 \cdot 10^{-2}$	1.14	$^{+2.8}_{-2.8}$	$^{+3.0}_{-2.1}$	$^{+1.2}_{-1.0}$	$^{-0.4}_{+0.3}$	$+0.1$	$^{+0.0}_{+0.3}$	$^{-0.9}_{+1.2}$	$^{+0.2}_{-1.2}$	$^{-1.1}_{+2.5}$
	$0.80 \cdot 10^{-2}$	0.95	$^{+2.7}_{-2.7}$	$^{+2.1}_{-1.6}$	$^{+1.3}_{-0.5}$	$^{-0.1}_{+0.3}$	$+0.0$	$^{+0.0}_{+0.0}$	$^{-1.1}_{+0.5}$	$^{+0.2}_{-0.8}$	$^{-0.6}_{+1.5}$
	$0.13 \cdot 10^{-1}$	0.82	$^{+2.8}_{-2.7}$	$^{+2.3}_{-1.9}$	$^{+1.0}_{-1.1}$	$^{-0.1}_{+0.1}$	$+0.1$	$^{+0.1}_{+0.2}$	$^{-0.7}_{-0.1}$	$^{+0.3}_{-1.0}$	$^{-0.9}_{+2.0}$
	$0.21 \cdot 10^{-1}$	0.70	$^{+3.4}_{-3.3}$	$^{+1.9}_{-1.5}$	$^{+1.5}_{-1.1}$	$^{-0.1}_{+0.3}$	-0.0	$^{+0.1}_{+0.0}$	$^{+0.1}_{-0.0}$	$^{+0.3}_{-0.8}$	$^{-0.5}_{+1.1}$
	$0.32 \cdot 10^{-1}$	0.59	$^{+3.5}_{-3.4}$	$^{+1.1}_{-2.1}$	$^{+0.9}_{-1.8}$	$^{-0.3}_{+0.3}$	-0.0	$^{-0.1}_{+0.1}$	$^{-0.3}_{+0.1}$	$^{+0.1}_{-0.9}$	$^{-0.1}_{+0.4}$
	$0.50 \cdot 10^{-1}$	0.50	$^{+3.3}_{-3.2}$	$^{+1.8}_{-2.5}$	$^{+1.5}_{-0.6}$	$^{-0.1}_{+0.3}$	$+0.1$	$^{+0.0}_{-0.1}$	$^{-0.1}_{-0.2}$	$^{+0.3}_{-1.1}$	$^{+0.9}_{-2.1}$
	$0.80 \cdot 10^{-1}$	0.42	$^{+2.9}_{-2.8}$	$^{+2.0}_{-3.5}$	$^{+1.3}_{-1.0}$	$^{-0.2}_{+0.3}$	$+0.2$	$^{+0.1}_{+0.0}$	$^{+0.1}_{+0.6}$	$^{+0.2}_{-1.0}$	$^{+1.3}_{-3.2}$
	0.18	0.32	$^{+3.9}_{-3.8}$	$^{+1.2}_{-3.9}$	$^{+0.8}_{-3.3}$	$^{-0.3}_{+0.0}$	$+0.0$	$^{+0.0}_{-0.0}$	$^{-0.4}_{-0.6}$	$^{+0.1}_{-1.2}$	$^{+0.8}_{-1.6}$
250	$0.50 \cdot 10^{-2}$	1.08	$^{+4.3}_{-4.2}$	$^{+3.4}_{-3.3}$	$^{+2.3}_{-2.4}$	$^{-1.3}_{+0.7}$	-0.6	$^{+0.0}_{-0.6}$	$^{+0.4}_{+1.3}$	$^{+0.0}_{-1.5}$	$^{-0.8}_{+1.9}$
	$0.80 \cdot 10^{-2}$	0.97	$^{+3.2}_{-3.2}$	$^{+1.9}_{-2.4}$	$^{+1.1}_{-1.5}$	$^{-0.3}_{+0.2}$	-0.1	$^{-0.1}_{-0.2}$	$^{-1.5}_{+0.9}$	$^{+0.1}_{-1.0}$	$^{-0.5}_{+1.3}$
	$0.13 \cdot 10^{-1}$	0.86	$^{+3.2}_{-3.2}$	$^{+2.2}_{-2.1}$	$^{+1.1}_{-1.0}$	$^{-0.1}_{+0.1}$	$+0.0$	$^{+0.0}_{+0.2}$	$^{-1.3}_{+0.7}$	$^{+0.3}_{-1.0}$	$^{-0.7}_{+1.7}$
	$0.21 \cdot 10^{-1}$	0.69	$^{+3.9}_{-3.8}$	$^{+0.8}_{-1.9}$	$^{+0.8}_{-1.4}$	$^{-0.1}_{-0.1}$	-0.1	$^{+0.1}_{+0.0}$	$^{-0.6}_{-0.7}$	$^{+0.2}_{-1.0}$	$^{+0.1}_{-0.0}$
	$0.32 \cdot 10^{-1}$	0.61	$^{+4.0}_{-3.9}$	$^{+1.3}_{-3.3}$	$^{+0.7}_{-1.5}$	$^{-0.1}_{+0.1}$	-0.0	$^{+0.1}_{-0.1}$	$^{-0.8}_{+0.4}$	$^{+0.1}_{-1.1}$	$^{+1.0}_{-2.6}$
	$0.50 \cdot 10^{-1}$	0.52	$^{+3.8}_{-3.7}$	$^{+1.8}_{-2.8}$	$^{+1.5}_{-1.0}$	$^{-0.3}_{+0.2}$	-0.0	$^{+0.0}_{+0.1}$	$^{-1.1}_{+0.4}$	$^{+0.1}_{-0.9}$	$^{+0.9}_{-2.1}$
	$0.80 \cdot 10^{-1}$	0.44	$^{+3.4}_{-3.3}$	$^{+1.7}_{-5.0}$	$^{+0.8}_{-2.8}$	$^{-0.3}_{+0.2}$	-0.1	$^{-0.2}_{-0.2}$	$^{-2.1}_{-0.4}$	$^{+0.2}_{-0.9}$	$^{+1.4}_{-3.4}$

Table 13: *Systematic uncertainties with bin-to-bin correlations for the reduced cross-section $\tilde{\sigma}(e^-p)$. The left part of the table contains the quoted Q^2 and x values, Q_c^2 and x_c, the measured cross-section $\tilde{\sigma}(e^-p)$ corrected to the Born level, the statistical error and the total systematic uncertainty. The right part of the table lists the total uncorrelated systematic uncertainty followed by the uncertainties δ_1–δ_6 (see text) with bin-to-bin correlations. For the latter, the upper (lower) numbers refer to positive (negative) variation of e.g. the cut value, whereas the signs of the numbers reflect the direction of change in the cross sections.*

Q_c^2 (GeV^2)	x_c	$\tilde{\sigma}(e^-p)$	stat. (%)	total sys. (%)	uncor. sys. (%)	δ_1 (%)	δ_2 (%)	δ_3 (%)	δ_4 (%)	δ_5 (%)	δ_6 (%)
	0.18	0.30	$^{+4.1}_{-4.0}$	$^{+6.9}_{-2.8}$	$^{+6.8}_{-2.2}$	$^{-0.1}_{-0.0}$	-0.0	$^{-0.2}_{-0.2}$	$^{-0.2}_{-0.2}$	$^{+0.1}_{-1.1}$	$^{+0.6}_{-1.4}$
350	$0.80 \cdot 10^{-2}$	0.98	$^{+4.6}_{-4.4}$	$^{+1.8}_{-1.7}$	$^{+1.2}_{-1.5}$	$^{+0.1}_{+0.2}$	$+0.0$	$^{+0.1}_{-0.3}$	$^{-0.1}_{+0.5}$	$^{+0.3}_{-0.7}$	$^{-0.4}_{+1.0}$
	$0.13 \cdot 10^{-1}$	0.85	$^{+3.8}_{-3.7}$	$^{+3.1}_{-2.2}$	$^{+1.2}_{-1.3}$	$^{-0.3}_{-0.1}$	-0.1	$^{-0.1}_{-0.0}$	$^{-0.5}_{-0.0}$	$^{-0.0}_{-1.2}$	$^{-1.2}_{+2.9}$
	$0.21 \cdot 10^{-1}$	0.72	$^{+4.3}_{-4.2}$	$^{+0.8}_{-2.7}$	$^{+0.7}_{-1.2}$	$^{-0.3}_{+0.1}$	$+0.0$	$^{-0.0}_{+0.1}$	$^{-2.1}_{+0.3}$	$^{+0.2}_{-1.1}$	$^{-0.0}_{+0.2}$
	$0.32 \cdot 10^{-1}$	0.59	$^{+4.5}_{-4.4}$	$^{+0.9}_{-2.2}$	$^{+0.8}_{-1.6}$	$^{-0.4}_{+0.0}$	-0.2	$^{+0.0}_{-0.2}$	$^{-0.4}_{-0.2}$	$^{+0.2}_{-1.3}$	$^{-0.2}_{+0.4}$
	$0.50 \cdot 10^{-1}$	0.53	$^{+4.3}_{-4.1}$	$^{+2.1}_{-1.2}$	$^{+1.4}_{-0.8}$	$^{+0.0}_{+0.5}$	$+0.0$	$^{+0.2}_{+0.2}$	$^{+1.2}_{+0.2}$	$^{+0.5}_{-0.8}$	$^{-0.2}_{+0.6}$
	$0.80 \cdot 10^{-1}$	0.44	$^{+3.8}_{-3.7}$	$^{+1.1}_{-2.2}$	$^{+0.6}_{-0.8}$	$^{-0.1}_{+0.4}$	$+0.1$	$^{-0.1}_{+0.1}$	$^{-0.6}_{-0.4}$	$^{+0.2}_{-0.9}$	$^{+0.8}_{-1.8}$
	0.18	0.31	$^{+4.2}_{-4.1}$	$^{+3.0}_{-2.7}$	$^{+2.9}_{-1.5}$	$^{-0.1}_{+0.2}$	-0.1	$^{-0.1}_{+0.1}$	$^{-1.6}_{-0.1}$	$^{+0.4}_{-0.9}$	$^{+0.4}_{-1.2}$
450	$0.80 \cdot 10^{-2}$	0.98	$^{+4.6}_{-4.5}$	$^{+2.1}_{-3.2}$	$^{+1.3}_{-1.4}$	$^{+0.0}_{+0.6}$	$+0.1$	$^{-0.0}_{+0.2}$	$^{-1.2}_{+0.9}$	$^{+0.8}_{-1.3}$	$^{+0.9}_{-2.3}$
	$0.13 \cdot 10^{-1}$	0.84	$^{+6.2}_{-5.9}$	$^{+4.5}_{-4.2}$	$^{+3.4}_{-2.6}$	$^{-0.3}_{-0.4}$	-0.2	$^{-0.4}_{-0.2}$	$^{-2.9}_{-0.8}$	$^{-0.2}_{-1.2}$	$^{-1.2}_{+2.9}$
	$0.21 \cdot 10^{-1}$	0.68	$^{+6.1}_{-5.8}$	$^{+2.7}_{-1.4}$	$^{+2.2}_{-1.0}$	$^{+0.1}_{+0.6}$	$+0.5$	$^{+0.4}_{+0.3}$	$^{+1.2}_{+0.2}$	$^{+0.5}_{-0.5}$	$^{+0.2}_{-0.8}$
	$0.32 \cdot 10^{-1}$	0.63	$^{+5.5}_{-5.3}$	$^{+1.9}_{-2.1}$	$^{+1.8}_{-1.5}$	$^{-0.1}_{+0.0}$	-0.0	$^{+0.1}_{+0.0}$	$^{-1.1}_{+0.2}$	$^{+0.3}_{-0.9}$	$^{+0.0}_{-0.2}$
	$0.50 \cdot 10^{-1}$	0.51	$^{+4.9}_{-4.8}$	$^{+1.8}_{-3.0}$	$^{+1.2}_{-1.0}$	$^{-0.1}_{+0.4}$	$+0.3$	$^{-0.0}_{+0.1}$	$^{+0.2}_{+0.0}$	$^{+0.3}_{-0.8}$	$^{+1.2}_{-2.7}$
	$0.80 \cdot 10^{-1}$	0.44	$^{+5.1}_{-4.9}$	$^{+1.8}_{-1.9}$	$^{+1.8}_{-1.3}$	$^{-0.5}_{+0.2}$	-0.2	$^{-0.1}_{-0.1}$	$^{+0.1}_{-0.2}$	$^{+0.2}_{-1.2}$	$^{+0.2}_{-0.5}$
	0.13	0.39	$^{+5.3}_{-5.1}$	$^{+1.6}_{-1.7}$	$^{+1.4}_{-0.8}$	$^{+0.2}_{+0.3}$	$+0.2$	$^{+0.3}_{+0.1}$	$^{-0.5}_{-0.4}$	$^{+0.5}_{-0.8}$	$^{+0.5}_{-1.2}$
	0.25	0.28	$^{+6.0}_{-5.7}$	$^{+2.3}_{-5.8}$	$^{+1.7}_{-5.7}$	$^{+0.1}_{+0.5}$	$+0.8$	$^{+0.7}_{+0.2}$	$^{-0.7}_{+0.8}$	$^{+0.5}_{-0.8}$	$^{-0.1}_{+0.4}$

Table 14: *Systematic uncertainties with bin-to-bin correlations for the reduced cross-section $\tilde{\sigma}(e^-p)$. The left part of the table contains the quoted Q^2 and x values, Q_c^2 and x_c, the measured cross-section $\tilde{\sigma}(e^-p)$ corrected to the Born level, the statistical error and the total systematic uncertainty. The right part of the table lists the total uncorrelated systematic uncertainty followed by the uncertainties δ_1–δ_6 (see text) with bin-to-bin correlations. For the latter, the upper (lower) numbers refer to positive (negative) variation of e.g. the cut value, whereas the signs of the numbers reflect the direction of change in the cross sections.*

Q_c^2 (GeV^2)	x_c	$\tilde{\sigma}(e^-p)$	stat. (%)	total sys. (%)	uncor. sys. (%)	δ_1 (%)	δ_2 (%)	δ_3 (%)	δ_4 (%)	δ_5 (%)	δ_6 (%)
650	$0.80 \cdot 10^{-2}$	0.90	$^{+6.2}_{-5.9}$	$^{+2.6}_{-2.5}$	$^{+2.1}_{-1.6}$	$^{-1.6}_{+1.4}$	$^{}_{+0.2}$	$^{-0.1}_{-0.0}$	$^{+0.1}_{-0.3}$	$^{-0.1}_{-1.0}$	$^{-0.3}_{+0.6}$
	$0.13 \cdot 10^{-1}$	0.92	$^{+4.6}_{-4.4}$	$^{+1.3}_{-3.1}$	$^{+0.6}_{-1.9}$	$^{-0.4}_{-0.0}$	$^{}_{-0.1}$	$^{-0.4}_{-0.4}$	$^{-2.0}_{+0.9}$	$^{+0.1}_{-1.2}$	$^{-0.3}_{+0.7}$
	$0.21 \cdot 10^{-1}$	0.79	$^{+6.7}_{-6.3}$	$^{+1.1}_{-2.2}$	$^{+0.9}_{-1.6}$	$^{-0.1}_{+0.2}$	$^{}_{-0.1}$	$^{-0.2}_{-0.1}$	$^{-1.0}_{-0.3}$	$^{+0.5}_{-0.9}$	$^{+0.4}_{-0.7}$
	$0.32 \cdot 10^{-1}$	0.60	$^{+8.6}_{-8.1}$	$^{+3.6}_{-1.2}$	$^{+3.4}_{-0.8}$	$^{-0.1}_{+0.1}$	$^{}_{+0.3}$	$^{+0.2}_{+0.7}$	$^{+0.1}_{+0.1}$	$^{+0.1}_{-0.8}$	$^{-0.5}_{+1.1}$
	$0.50 \cdot 10^{-1}$	0.50	$^{+8.4}_{-7.9}$	$^{+2.7}_{-3.5}$	$^{+1.6}_{-3.4}$	$^{+0.2}_{+0.0}$	$^{}_{-0.2}$	$^{-0.3}_{+0.2}$	$^{-0.2}_{+2.0}$	$^{+0.4}_{-0.6}$	$^{-0.3}_{+0.8}$
	$0.80 \cdot 10^{-1}$	0.40	$^{+8.6}_{-8.0}$	$^{+1.9}_{-2.5}$	$^{+1.8}_{-2.2}$	$^{+0.1}_{+0.2}$	$^{}_{-0.1}$	$^{+0.0}_{+0.2}$	$^{-0.5}_{+0.3}$	$^{+0.2}_{-0.2}$	$^{+0.4}_{-1.0}$
	0.13	0.35	$^{+8.2}_{-7.7}$	$^{+1.8}_{-3.4}$	$^{+1.7}_{-2.7}$	$^{-0.6}_{+0.1}$	$^{}_{-0.5}$	$^{-0.4}_{-0.4}$	$^{+0.3}_{+0.1}$	$^{-0.3}_{-1.1}$	$^{+0.6}_{-1.5}$
	0.25	0.26	$^{+8.3}_{-7.8}$	$^{+5.7}_{-3.6}$	$^{+5.6}_{-2.6}$	$^{-0.1}_{+0.2}$	$^{}_{-0.3}$	$^{+0.0}_{+0.1}$	$^{-0.5}_{-0.3}$	$^{+0.2}_{-0.8}$	$^{+1.0}_{-2.4}$
800	$0.13 \cdot 10^{-1}$	0.86	$^{+5.6}_{-5.3}$	$^{+3.2}_{-1.2}$	$^{+2.4}_{-1.0}$	$^{+0.6}_{+0.7}$	$^{}_{-0.0}$	$^{+0.2}_{+0.4}$	$^{+0.4}_{+1.7}$	$^{+1.1}_{-0.5}$	$^{+0.2}_{-0.4}$
	$0.21 \cdot 10^{-1}$	0.80	$^{+6.9}_{-6.5}$	$^{+1.8}_{-2.5}$	$^{+1.7}_{-1.7}$	$^{+0.1}_{+0.2}$	$^{}_{-0.0}$	$^{+0.1}_{+0.1}$	$^{-0.6}_{-0.7}$	$^{+0.4}_{-1.1}$	$^{+0.5}_{-1.2}$
	$0.32 \cdot 10^{-1}$	0.63	$^{+7.3}_{-6.9}$	$^{+1.9}_{-4.3}$	$^{+0.8}_{-1.2}$	$^{+0.1}_{+0.1}$	$^{}_{-0.1}$	$^{-0.1}_{-0.4}$	$^{-0.7}_{+0.1}$	$^{+0.3}_{-1.0}$	$^{+1.7}_{-3.9}$
	$0.50 \cdot 10^{-1}$	0.58	$^{+7.0}_{-6.6}$	$^{+1.5}_{-2.4}$	$^{+1.2}_{-0.9}$	$^{-0.3}_{+0.1}$	$^{}_{-0.3}$	$^{+0.1}_{-0.1}$	$^{-0.3}_{-0.2}$	$^{+0.3}_{-0.9}$	$^{+0.8}_{-1.9}$
	$0.80 \cdot 10^{-1}$	0.49	$^{+8.0}_{-7.6}$	$^{+1.3}_{-3.8}$	$^{+0.6}_{-3.1}$	$^{-0.3}_{-0.3}$	$^{}_{-0.5}$	$^{-0.8}_{-0.6}$	$^{-1.3}_{-1.0}$	$^{+0.2}_{-1.2}$	$^{-0.5}_{+1.2}$
	0.13	0.34	$^{+9.7}_{-9.0}$	$^{+3.1}_{-6.7}$	$^{+1.8}_{-2.8}$	$^{-0.4}_{-0.2}$	$^{}_{-0.3}$	$^{-0.6}_{-0.5}$	$^{-1.6}_{-1.7}$	$^{-0.4}_{-1.2}$	$^{+2.6}_{-5.7}$
	0.25	0.26	$^{+12.}_{-11.}$	$^{+6.7}_{-2.0}$	$^{+4.9}_{-0.5}$	$^{+0.4}_{+1.1}$	$^{}_{+0.0}$	$^{-0.2}_{+0.4}$	$^{-0.3}_{+0.6}$	$^{+0.7}_{-0.2}$	$^{-1.9}_{+4.3}$

Table 15: *Systematic uncertainties with bin-to-bin correlations for the reduced cross-section $\tilde{\sigma}(e^-p)$. The left part of the table contains the quoted Q^2 and x values, Q_c^2 and x_c, the measured cross-section $\tilde{\sigma}(e^-p)$ corrected to the Born level, the statistical error and the total systematic uncertainty. The right part of the table lists the total uncorrelated systematic uncertainty followed by the uncertainties δ_1–δ_6 (see text) with bin-to-bin correlations. For the latter, the upper (lower) numbers refer to positive (negative) variation of e.g. the cut value, whereas the signs of the numbers reflect the direction of change in the cross sections.*

Q_c^2 (GeV^2)	x_c	$\tilde{\sigma}(e^-p)$	stat. (%)	total sys. (%)	uncor. sys. (%)	δ_1 (%)	δ_2 (%)	δ_3 (%)	δ_4 (%)	δ_5 (%)	δ_6 (%)
1200	$0.14 \cdot 10^{-1}$	0.87	$^{+6.7}_{-6.3}$	$^{+7.0}_{-2.7}$	$^{+3.3}_{-0.7}$	$^{-0.1}_{+0.4}$	-2.0	$^{+0.9}_{-0.4}$	$^{-0.7}_{+5.4}$	$^{+0.2}_{-0.7}$	$^{-1.3}_{+3.0}$
	$0.21 \cdot 10^{-1}$	0.67	$^{+7.3}_{-6.9}$	$^{+1.8}_{-1.6}$	$^{+1.6}_{-1.1}$	$^{+0.2}_{+0.4}$	$+0.1$	$^{+0.3}_{-0.6}$	$^{-0.1}_{-0.0}$	$^{+0.4}_{-0.7}$	$^{+0.3}_{-0.8}$
	$0.32 \cdot 10^{-1}$	0.58	$^{+7.2}_{-6.8}$	$^{+1.1}_{-3.0}$	$^{+1.1}_{-2.1}$	$^{-0.2}_{-0.2}$	$+0.1$	$^{-0.2}_{+0.1}$	$^{-1.8}_{-0.2}$	$^{+0.2}_{-1.3}$	$^{-0.1}_{+0.2}$
	$0.50 \cdot 10^{-1}$	0.51	$^{+6.4}_{-6.1}$	$^{+2.4}_{-1.0}$	$^{+1.9}_{-0.8}$	$^{+0.2}_{+0.5}$	$+0.3$	$^{+0.2}_{+0.5}$	$^{+1.1}_{+1.0}$	$^{+0.5}_{-0.5}$	$^{-0.0}_{+0.2}$
	$0.80 \cdot 10^{-1}$	0.43	$^{+6.6}_{-6.3}$	$^{+1.7}_{-2.3}$	$^{+1.6}_{-1.2}$	$^{-0.1}_{+0.1}$	$+0.1$	$^{-0.1}_{-0.2}$	$^{-1.1}_{-0.1}$	$^{+0.3}_{-1.1}$	$^{+0.5}_{-1.2}$
	0.13	0.36	$^{+7.0}_{-6.6}$	$^{+3.3}_{-1.4}$	$^{+2.9}_{-0.4}$	$^{+0.3}_{+0.1}$	$+0.2$	$^{+0.2}_{+0.4}$	$^{-0.7}_{+1.3}$	$^{+0.5}_{-1.0}$	$^{+0.2}_{-0.6}$
	0.25	0.27	$^{+7.8}_{-7.3}$	$^{+1.5}_{-2.1}$	$^{+1.3}_{-1.7}$	$^{+0.2}_{+0.0}$	$+0.0$	$^{+0.2}_{-0.1}$	$^{+0.3}_{-0.3}$	$^{+0.5}_{-1.1}$	$^{+0.3}_{-0.2}$
	0.40	0.10	$^{+15.}_{-13.}$	$^{+4.1}_{-18.}$	$^{+1.8}_{-17.}$	$^{-0.2}_{+0.8}$	$+0.1$	$^{+0.8}_{-0.2}$	$^{+3.1}_{+0.2}$	$^{+0.4}_{-0.9}$	$^{+1.6}_{-3.7}$
1500	$0.21 \cdot 10^{-1}$	0.79	$^{+9.1}_{-8.4}$	$^{+4.1}_{-2.2}$	$^{+2.6}_{-2.0}$	$^{+0.3}_{+0.7}$	$+1.6$	$^{+0.6}_{-0.3}$	$^{-0.6}_{+2.3}$	$^{+0.5}_{-0.5}$	$^{-0.3}_{+0.7}$
	$0.32 \cdot 10^{-1}$	0.74	$^{+8.5}_{-7.9}$	$^{+2.4}_{-1.6}$	$^{+0.9}_{-0.6}$	$^{-0.1}_{+0.3}$	-0.2	$^{-0.1}_{+0.8}$	$^{+1.8}_{-1.2}$	$^{+0.2}_{-0.7}$	$^{-0.4}_{+1.0}$
	$0.50 \cdot 10^{-1}$	0.60	$^{+7.7}_{-7.2}$	$^{+0.8}_{-2.4}$	$^{+0.4}_{-1.1}$	$^{-0.2}_{-0.0}$	-0.2	$^{-0.2}_{-0.1}$	$^{-1.6}_{+0.3}$	$^{+0.4}_{-1.0}$	$^{+0.5}_{-1.1}$
	$0.80 \cdot 10^{-1}$	0.44	$^{+8.4}_{-7.8}$	$^{+1.2}_{-2.7}$	$^{+0.9}_{-1.5}$	$^{-0.3}_{-0.3}$	$+0.0$	$^{-0.3}_{-0.4}$	$^{-1.3}_{+0.6}$	$^{+0.1}_{-1.4}$	$^{+0.4}_{-0.9}$
	0.13	0.40	$^{+9.9}_{-9.1}$	$^{+3.1}_{-2.9}$	$^{+0.9}_{-2.2}$	$^{-0.3}_{-0.1}$	$+0.0$	$^{-0.2}_{+0.1}$	$^{+0.1}_{-0.6}$	$^{+0.1}_{-1.2}$	$^{-1.2}_{+2.9}$
	0.18	0.33	$^{+10.}_{-9.4}$	$^{+2.9}_{-1.1}$	$^{+2.5}_{-0.4}$	$^{+0.3}_{+0.4}$	$+0.6$	$^{+0.1}_{+0.7}$	$^{-0.8}_{+0.9}$	$^{+0.5}_{-0.5}$	$^{-0.3}_{+0.5}$
	0.25	0.27	$^{+13.}_{-11.}$	$^{+2.6}_{-0.8}$	$^{+2.4}_{-0.3}$	$^{+0.0}_{+0.6}$	$+0.3$	$^{+0.4}_{+0.5}$	$^{-0.1}_{+0.0}$	$^{+0.4}_{-0.5}$	$^{+0.2}_{-0.5}$
	0.40	0.14	$^{+20.}_{-17.}$	$^{+38.}_{-9.0}$	$^{+38.}_{-8.8}$	$^{-0.9}_{-0.2}$	$+0.2$	$^{-0.3}_{+0.5}$	$^{-0.9}_{+0.5}$	$^{-0.4}_{-1.2}$	$^{-0.8}_{+1.5}$

Table 16: *Systematic uncertainties with bin-to-bin correlations for the reduced cross-section $\tilde{\sigma}(e^-p)$. The left part of the table contains the quoted Q^2 and x values, Q_c^2 and x_c, the measured cross-section $\tilde{\sigma}(e^-p)$ corrected to the Born level, the statistical error and the total systematic uncertainty. The right part of the table lists the total uncorrelated systematic uncertainty followed by the uncertainties δ_1–δ_6 (see text) with bin-to-bin correlations. For the latter, the upper (lower) numbers refer to positive (negative) variation of e.g. the cut value, whereas the signs of the numbers reflect the direction of change in the cross sections.*

Q_c^2 (GeV^2)	x_c	$\tilde{\sigma}(e^-p)$	stat. (%)	total sys. (%)	uncor. sys. (%)	δ_1 (%)	δ_2 (%)	δ_3 (%)	δ_4 (%)	δ_5 (%)	δ_6 (%)
2000	$0.32 \cdot 10^{-1}$	0.69	$^{+10.}_{-9.3}$	$^{+6.3}_{-1.6}$	$^{+5.3}_{-0.8}$	$^{+0.8}_{+1.0}$	-1.4	$^{+1.8}_{+1.0}$	$^{+0.8}_{+2.6}$	$^{+1.2}_{+0.1}$	$^{-0.0}_{-0.0}$
	$0.50 \cdot 10^{-1}$	0.54	$^{+10.}_{-9.3}$	$^{+1.8}_{-3.1}$	$^{+1.0}_{-1.5}$	$^{-0.0}_{+0.1}$	$+0.2$	$^{+0.1}_{-0.4}$	$^{+0.9}_{+0.2}$	$^{+0.4}_{-0.9}$	$^{+1.1}_{-2.5}$
	$0.80 \cdot 10^{-1}$	0.43	$^{+10.}_{-9.3}$	$^{+2.5}_{-4.7}$	$^{+0.9}_{-2.8}$	$^{+0.0}_{-0.0}$	$+0.0$	$^{+0.0}_{+0.1}$	$^{+1.6}_{+1.2}$	$^{+0.4}_{-1.2}$	$^{+1.6}_{-3.6}$
	0.13	0.38	$^{+12.}_{-11.}$	$^{+4.3}_{-1.8}$	$^{+4.3}_{-1.4}$	$^{+0.2}_{-0.0}$	-0.2	$^{-0.1}_{+0.2}$	$^{-0.2}_{+0.3}$	$^{+0.4}_{-1.0}$	$^{+0.3}_{-0.6}$
	0.18	0.28	$^{+13.}_{-12.}$	$^{+3.3}_{-2.8}$	$^{+3.2}_{-0.9}$	$^{-0.2}_{+0.1}$	$+0.1$	$^{+0.1}_{+0.0}$	$^{-1.0}_{-0.3}$	$^{+0.1}_{-0.9}$	$^{+1.0}_{-2.3}$
	0.25	0.29	$^{+14.}_{-13.}$	$^{+2.5}_{-3.0}$	$^{+2.2}_{-2.5}$	$^{+0.5}_{+0.6}$	$+0.3$	$^{-0.1}_{+0.3}$	$^{-0.5}_{+0.0}$	$^{+0.5}_{-0.5}$	$^{+0.7}_{-1.6}$
	0.40	0.10	$^{+24.}_{-20.}$	$^{+9.7}_{-7.4}$	$^{+9.1}_{-3.2}$	$^{-1.0}_{-0.5}$	-1.0	$^{-0.7}_{-0.7}$	$^{-1.4}_{+2.1}$	$^{-0.5}_{-2.4}$	$^{+2.6}_{-5.9}$
3000	$0.50 \cdot 10^{-1}$	0.66	$^{+12.}_{-10.}$	$^{+2.9}_{-4.2}$	$^{+1.3}_{-1.3}$	$^{+0.2}_{+0.4}$	$+0.8$	$^{-0.3}_{+1.2}$	$^{-3.8}_{+2.1}$	$^{+0.4}_{-0.7}$	$^{+0.3}_{-0.9}$
	$0.80 \cdot 10^{-1}$	0.45	$^{+12.}_{-11.}$	$^{+2.4}_{-3.2}$	$^{+1.5}_{-0.7}$	$^{-0.0}_{+0.0}$	-0.1	$^{-0.2}_{+0.3}$	$^{+1.3}_{+1.0}$	$^{+0.2}_{-1.1}$	$^{+1.2}_{-2.9}$
	0.13	0.37	$^{+15.}_{-13.}$	$^{+2.8}_{-7.3}$	$^{+2.1}_{-7.3}$	$^{+0.3}_{+0.5}$	$+0.4$	$^{+0.6}_{+0.4}$	$^{+1.5}_{+0.1}$	$^{+0.6}_{-0.8}$	$^{+0.2}_{-0.4}$
	0.18	0.30	$^{+16.}_{-14.}$	$^{+3.2}_{-2.2}$	$^{+2.8}_{-2.0}$	$^{+0.0}_{+0.1}$	$+0.2$	$^{+0.1}_{+0.1}$	$^{+0.9}_{-0.5}$	$^{+0.6}_{-0.8}$	$^{-0.4}_{+1.2}$
	0.25	0.28	$^{+17.}_{-15.}$	$^{+4.4}_{-4.6}$	$^{+0.7}_{-3.4}$	$^{-0.1}_{+0.0}$	-0.4	$^{-0.6}_{+0.0}$	$^{+0.8}_{-2.3}$	$^{+0.2}_{-1.1}$	$^{-1.8}_{+4.2}$
	0.40	0.16	$^{+25.}_{-21.}$	$^{+6.3}_{-6.6}$	$^{+4.9}_{-6.0}$	$^{-0.3}_{-0.3}$	-0.3	$^{-0.9}_{+0.8}$	$^{+1.1}_{-0.9}$	$^{+0.2}_{-1.6}$	$^{-1.6}_{+3.7}$
	0.65	0.02	$^{+51.}_{-36.}$	$^{+9.4}_{-5.8}$	$^{+8.8}_{-4.6}$	$^{+0.0}_{+2.1}$	$+1.0$	$^{-0.1}_{+1.0}$	$^{+1.2}_{+1.5}$	$^{+0.3}_{-0.1}$	$^{+1.5}_{-3.5}$

Table 17: *Systematic uncertainties with bin-to-bin correlations for the reduced cross-section $\tilde{\sigma}(e^-p)$. The left part of the table contains the quoted Q^2 and x values, Q_c^2 and x_c, the measured cross-section $\tilde{\sigma}(e^-p)$ corrected to the Born level, the statistical error and the total systematic uncertainty. The right part of the table lists the total uncorrelated systematic uncertainty followed by the uncertainties δ_1–δ_6 (see text) with bin-to-bin correlations. For the latter, the upper (lower) numbers refer to positive (negative) variation of e.g. the cut value, whereas the signs of the numbers reflect the direction of change in the cross sections.*

Q_c^2 (GeV^2)	x_c	$\tilde{\sigma}(e^-p)$	stat. (%)	total sys. (%)	uncor. sys. (%)	δ_1 (%)	δ_2 (%)	δ_3 (%)	δ_4 (%)	δ_5 (%)	δ_6 (%)
5000	$0.80 \cdot 10^{-1}$	0.59	$^{+9.9}_{-9.1}$	$^{+3.3}_{-1.2}$	$^{+2.4}_{-0.6}$	$^{+0.4}_{+0.6}$	-0.7	$^{+0.5}_{+0.3}$	$^{+0.3}_{+2.0}$	$^{+0.7}_{-0.6}$	$^{+0.1}_{-0.2}$
	0.13	0.44	$^{+15.}_{-13.}$	$^{+2.8}_{-1.9}$	$^{+2.8}_{-0.4}$	$^{+0.2}_{+0.3}$	$+0.1$	$^{+0.1}_{-1.4}$	$^{-1.0}_{-0.2}$	$^{+0.3}_{-0.8}$	$^{-0.1}_{+0.1}$
	0.18	0.41	$^{+14.}_{-13.}$	$^{+3.2}_{-3.4}$	$^{+2.8}_{-1.4}$	$^{-0.1}_{+0.1}$	$+0.0$	$^{+0.3}_{+0.6}$	$^{+0.7}_{-0.0}$	$^{+0.3}_{-0.8}$	$^{+1.3}_{-3.0}$
	0.25	0.27	$^{+18.}_{-16.}$	$^{+1.8}_{-2.9}$	$^{+1.3}_{-0.5}$	$^{+0.0}_{-0.3}$	$+0.1$	$^{+0.4}_{+0.1}$	$^{+0.6}_{+0.1}$	$^{+0.2}_{-1.3}$	$^{+1.1}_{-2.5}$
	0.40	0.16	$^{+25.}_{-20.}$	$^{+3.7}_{-11.}$	$^{+3.4}_{-7.0}$	$^{-0.4}_{+0.9}$	$+0.7$	$^{+0.2}_{-3.1}$	$^{-7.1}_{+0.2}$	$^{+0.2}_{-0.6}$	$^{-0.1}_{+0.3}$
8000	0.13	0.53	$^{+15.}_{-13.}$	$^{+3.0}_{-4.9}$	$^{+0.7}_{-3.7}$	$^{-0.5}_{+0.2}$	-2.0	$^{+2.4}_{+2.5}$	$^{-2.1}_{+1.4}$	$^{+0.2}_{-1.0}$	$^{+0.3}_{-0.6}$
	0.18	0.38	$^{+20.}_{-17.}$	$^{+3.5}_{-4.1}$	$^{+2.0}_{-3.2}$	$^{-0.1}_{+0.1}$	-0.1	$^{-0.1}_{+0.1}$	$^{+0.4}_{+2.7}$	$^{+0.1}_{-1.1}$	$^{+0.9}_{-2.2}$
	0.25	0.31	$^{+24.}_{-19.}$	$^{+2.1}_{-1.5}$	$^{+1.3}_{-0.5}$	$^{+0.1}_{+0.1}$	$+0.4$	$^{+0.1}_{+0.8}$	$^{+1.2}_{-0.1}$	$^{+0.4}_{-0.9}$	$^{+0.5}_{-1.1}$
	0.40	0.14	$^{+37.}_{-28.}$	$^{+5.8}_{-7.9}$	$^{+2.6}_{-1.3}$	$^{-0.2}_{+0.3}$	$+0.0$	$^{+0.5}_{+0.1}$	$^{-7.5}_{-0.8}$	$^{+0.1}_{-0.8}$	$^{-2.2}_{+5.1}$
	0.65	0.02	$^{+80.}_{-48.}$	$^{+7.4}_{-1.8}$	$^{+7.2}_{-1.4}$	$^{+0.1}_{+0.0}$	$+0.0$	$^{+0.4}_{+0.4}$	$^{+0.6}_{+0.8}$	$^{+0.5}_{-1.0}$	$^{-0.6}_{+1.1}$
12000	0.18	0.45	$^{+22.}_{-18.}$	$^{+6.4}_{-2.9}$	$^{+3.4}_{-0.9}$	$^{-0.7}_{+0.7}$	$+3.4$	$^{-1.1}_{+3.0}$	$^{-1.7}_{+2.9}$	$^{+0.2}_{-1.1}$	$^{+0.6}_{-1.3}$
	0.25	0.27	$^{+37.}_{-28.}$	$^{+3.1}_{-8.3}$	$^{+1.1}_{-8.2}$	$^{-0.1}_{+0.1}$	$+0.2$	$^{-0.6}_{+0.8}$	$^{+0.4}_{-0.2}$	$^{+0.1}_{-0.9}$	$^{-1.2}_{+2.8}$
	0.40	0.11	$^{+60.}_{-40.}$	$^{+17.}_{-0.5}$	$^{+17.}_{-0.1}$	$^{+0.2}_{+0.9}$	$+0.2$	$^{+0.2}_{+0.9}$	$^{+0.6}_{+0.4}$	$^{+0.5}_{-0.1}$	$^{-0.5}_{+1.3}$
20000	0.25	0.43	$^{+35.}_{-27.}$	$^{+5.7}_{-2.0}$	$^{+1.2}_{-0.8}$	$^{-0.6}_{+0.3}$	$+0.0$	$^{-1.2}_{+4.6}$	$^{+3.1}_{-0.6}$	$^{+0.2}_{-1.1}$	$^{+0.1}_{-0.1}$
	0.40	0.21	$^{+60.}_{-40.}$	$^{+3.4}_{-2.0}$	$^{+2.4}_{-1.1}$	$^{-0.4}_{+0.2}$	-0.1	$^{-1.1}_{+2.1}$	$^{+1.1}_{-0.2}$	$^{+0.2}_{-1.2}$	$^{-0.1}_{+0.3}$
30000	0.40	0.23	$^{+80.}_{-48.}$	$^{+11.}_{-2.3}$	$^{+0.8}_{-0.7}$	$^{-0.5}_{+0.8}$	$+9.6$	$^{-1.7}_{+4.7}$	$^{+2.5}_{-0.3}$	$^{+0.2}_{-0.9}$	$^{-1.0}_{+2.2}$

Table 18: *Systematic uncertainties with bin-to-bin correlations for the reduced cross-section $\tilde{\sigma}(e^-p)$. The left part of the table contains the quoted Q^2 and x values, Q_c^2 and x_c, the measured cross-section $\tilde{\sigma}(e^-p)$ corrected to the Born level, the statistical error and the total systematic uncertainty. The right part of the table lists the total uncorrelated systematic uncertainty followed by the uncertainties δ_1–δ_6 (see text) with bin-to-bin correlations. For the latter, the upper (lower) numbers refer to positive (negative) variation of e.g. the cut value, whereas the signs of the numbers reflect the direction of change in the cross sections.*

Q^2 range (GeV^2)	x range	Q_c^2 (GeV^2)	x_c	xF_3		N_{e^-p}	N_{e^+p}
				measured	SM		
1300 – 2500	0.017 – 0.060	1500	0.050	$(10.6 \pm 4.0\,^{+2.2}_{-1.3}) \cdot 10^{-2}$	$3.7 \cdot 10^{-2}$	783	1112
	0.060 – 0.230		0.130	$(\ 4.1 \pm 7.4\,^{+3.2}_{-2.7}) \cdot 10^{-2}$	$4.4 \cdot 10^{-2}$	719	1230
	0.230 – 0.530		0.400	$(-0.5\,^{+1.6}_{-1.5}\ ^{+0.6}_{-1.4}) \cdot 10^{-1}$	$0.2 \cdot 10^{-1}$	213	373
2500 – 3500	0.037 – 0.060	3000	0.050	$(\ 7.2\,^{+6.1}_{-5.6}\ ^{+1.9}_{-2.0}) \cdot 10^{-2}$	$6.6 \cdot 10^{-2}$	95	140
	0.060 – 0.230		0.130	$(\ 6.0\,^{+6.6}_{-6.2}\ ^{+2.6}_{-1.3}) \cdot 10^{-2}$	$7.6 \cdot 10^{-2}$	200	321
	0.230 – 0.750		0.400	$(\ 3.0\,^{+1.4}_{-1.3}\ ^{+0.3}_{-1.0}) \cdot 10^{-1}$	$0.3 \cdot 10^{-1}$	77	93
3500 – 5600	0.040 – 0.230	5000	0.130	$(16.5\,^{+3.9}_{-3.7}\ ^{+1.7}_{-0.9}) \cdot 10^{-2}$	$10.8 \cdot 10^{-2}$	253	296
	0.230 – 0.530		0.400	$(\ 7.5\,^{+8.7}_{-7.7}\ ^{+3.0}_{-2.5}) \cdot 10^{-2}$	$4.7 \cdot 10^{-2}$	65	91
5600 – 9000	0.070 – 0.230	8000	0.180	$(15.2\,^{+4.9}_{-4.4}\ ^{+1.9}_{-1.4}) \cdot 10^{-2}$	$13.4 \cdot 10^{-2}$	94	91
	0.230 – 0.750		0.400	$(\ 4.6\,^{+6.8}_{-5.8}\ ^{+1.3}_{-1.7}) \cdot 10^{-2}$	$6.0 \cdot 10^{-2}$	42	60
9000 – 15000	0.110 – 0.230	12000	0.180	$(12.8\,^{+6.8}_{-5.7}\ ^{+2.1}_{-0.9}) \cdot 10^{-2}$	$16.0 \cdot 10^{-2}$	29	25
	0.230 – 0.530		0.400	$(\ 3.8\,^{+5.9}_{-4.6}\ ^{+1.1}_{-1.5}) \cdot 10^{-2}$	$7.1 \cdot 10^{-2}$	18	22
15000 – 50000	0.180 – 0.750	30000	0.400	$(\ 9.2\,^{+3.3}_{-2.7}\ ^{+0.7}_{-0.3}) \cdot 10^{-2}$	$9.0 \cdot 10^{-2}$	23	13

Table 19: *The structure function xF_3 for the reaction $e^{\pm}p \to e^{\pm}X$. The following quantities are given for each bin: the Q^2 and x ranges, the values at which xF_3 is quoted, Q_c^2 and x_c, the value of the measured structure function and the xF_3 value predicted by the SM using CTEQ5D PDFs. The first error of the measured value gives the statistical error and the second is the systematic uncertainty. The last two columns contain the number of events in each of the e^-p and e^+p data samples.*

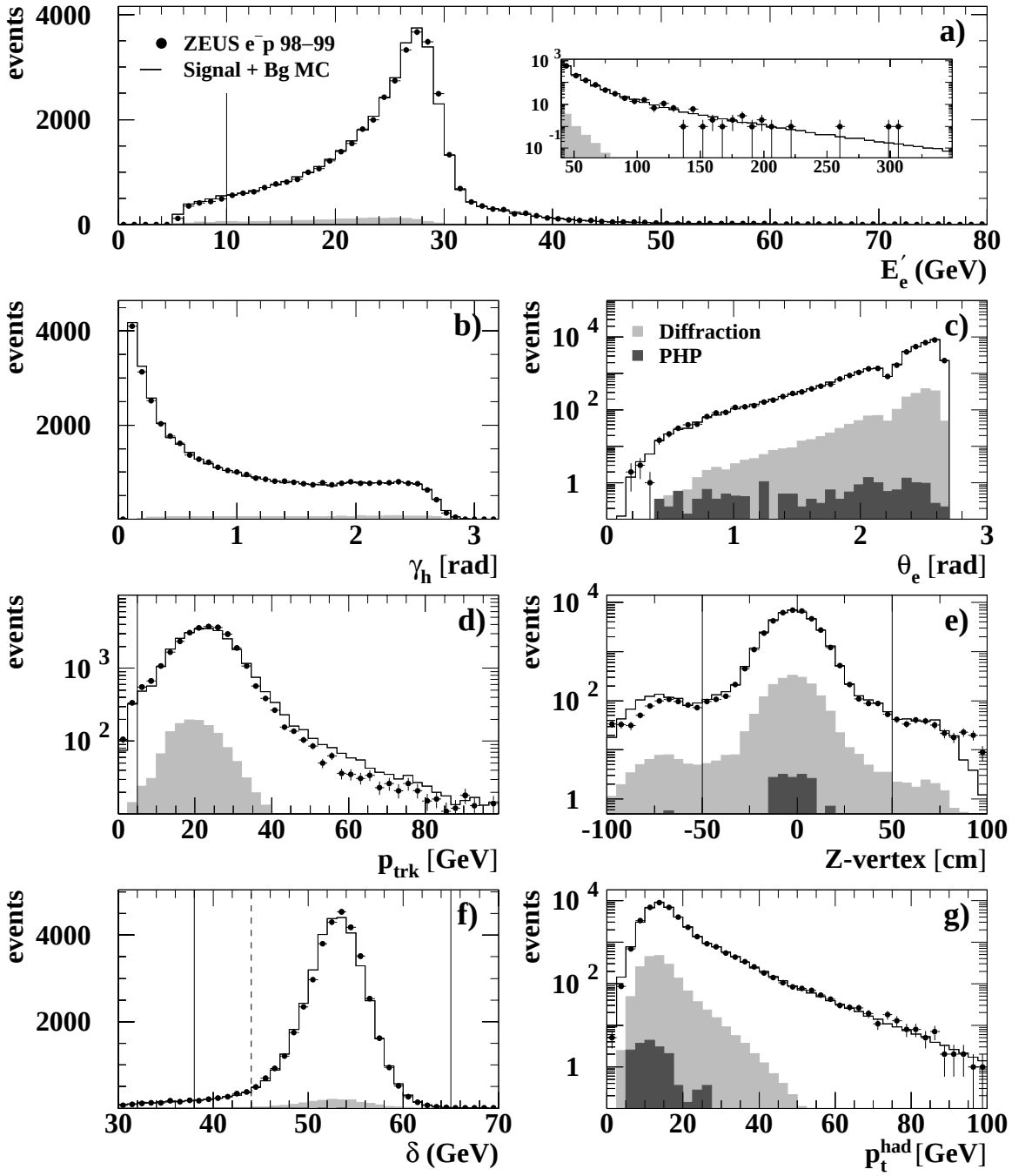

Figure 1: *Comparison of e^-p data (points) and MC simulation (histograms) for a) E'_e, the energy of the scattered electron (the inset shows the high-energy part of the distribution), b) γ_h, the angle of the hadronic system, c) θ_e, the angle of the scattered electron, d) $p_{\rm trk}$, the momentum of the track matched to the electron, e) Z coordinate of the event vertex, f) $\delta = \sum_i (E - p_Z)_i$ and g) $p_t^{\rm had}$, the transverse momentum of the hadronic system. The darkest shaded area shows the PHP contribution. The histogram shows the sum of the background and the diffractive (lightest shading) and the non-diffractive NC signal MC samples. The vertical lines indicate the cut boundaries described in the text (the dashed line represents the tightened cut for electrons outside the forward CTD acceptance).*

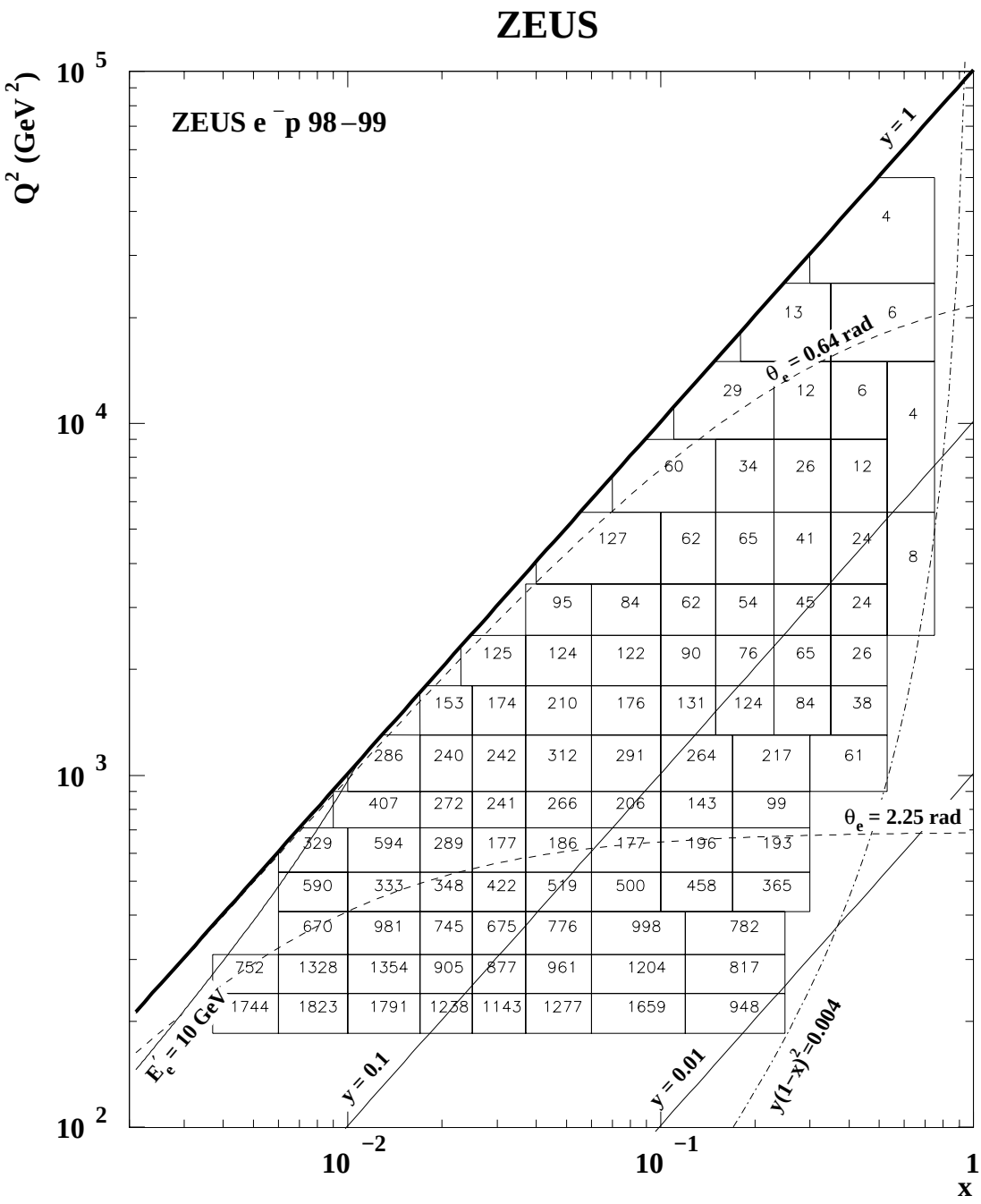

Figure 2: *Double-differential bins at $\sqrt{s} = 318\ GeV$ in the x-Q^2 plane. The heavy solid line $y = 1$ marks the kinematic limit. The two solid diagonal lines are lines at $y = 0.1$ and $y = 0.01$, whereas the curved line is a line at $E'_e = 10\ GeV$. The dashed lines are lines of constant θ_e and mark the transition regions between R/BCAL ($\theta_e = 2.25\ rad$) and B/FCAL ($\theta_e = 0.64\ rad$). The dash-dotted line $y(1-x)^2 = 0.004$ indicates the validity limit of the MC simulation. The number of data events is displayed in each bin.*

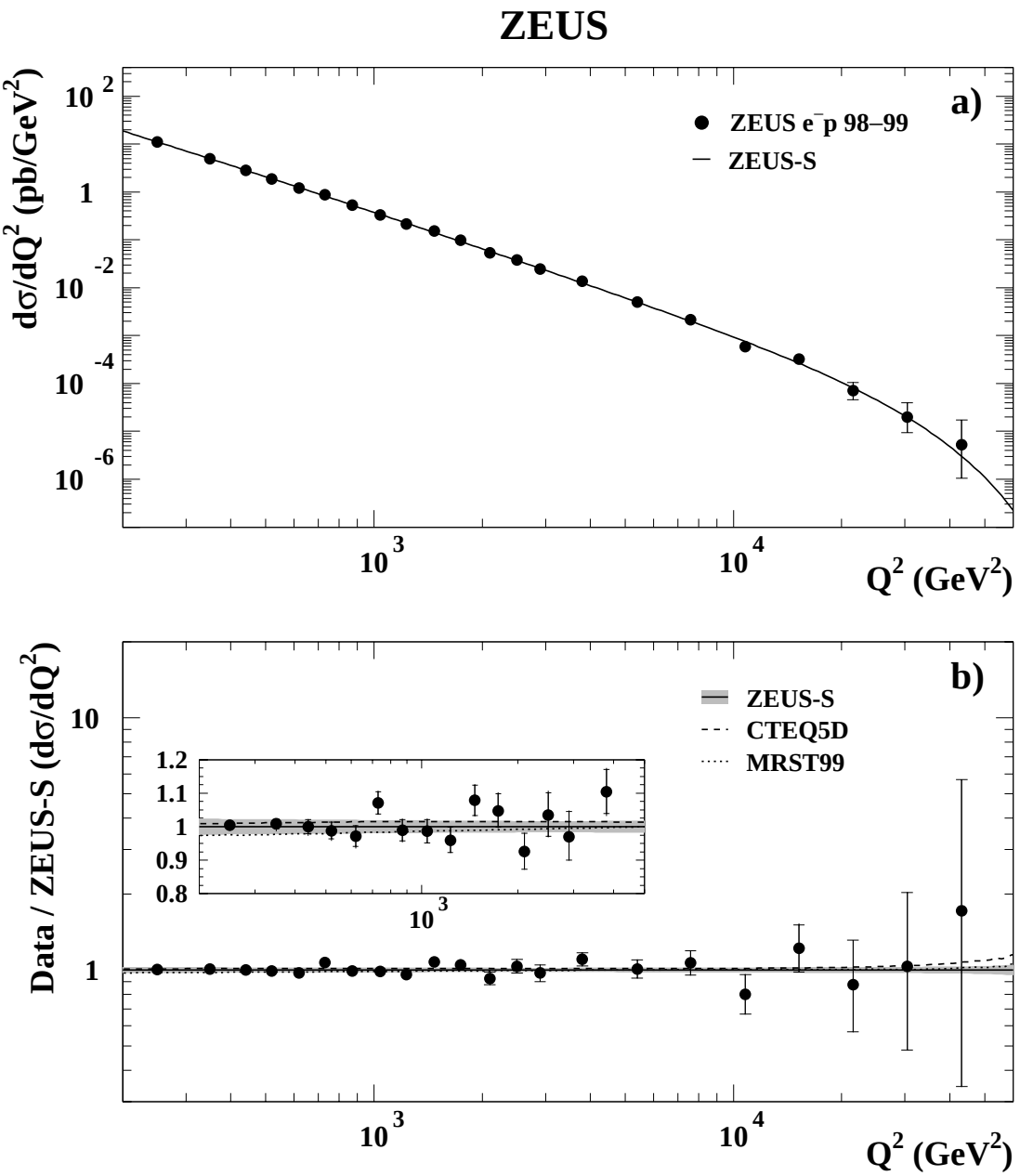

Figure 3: *a) The differential e^-p cross-section $d\sigma/dQ^2$ as a function of Q^2 compared to the SM expectation evaluated using the ZEUS-S fit. b) The ratio of the measured cross section to the ZEUS-S prediction. Also shown are the ratios of the SM prediction using CTEQ5D and MRST99 PDFs to that of ZEUS-S. The inset shows the range $200 < Q^2 < 5\,000\ GeV^2$ on a linear y scale. The shaded band indicates the uncertainty on the calculated cross section due to the uncertainty in the ZEUS-S PDFs. The inner error bars of the measured points show the statistical uncertainty, while the outer ones show the statistical and systematic uncertainties added in quadrature.*

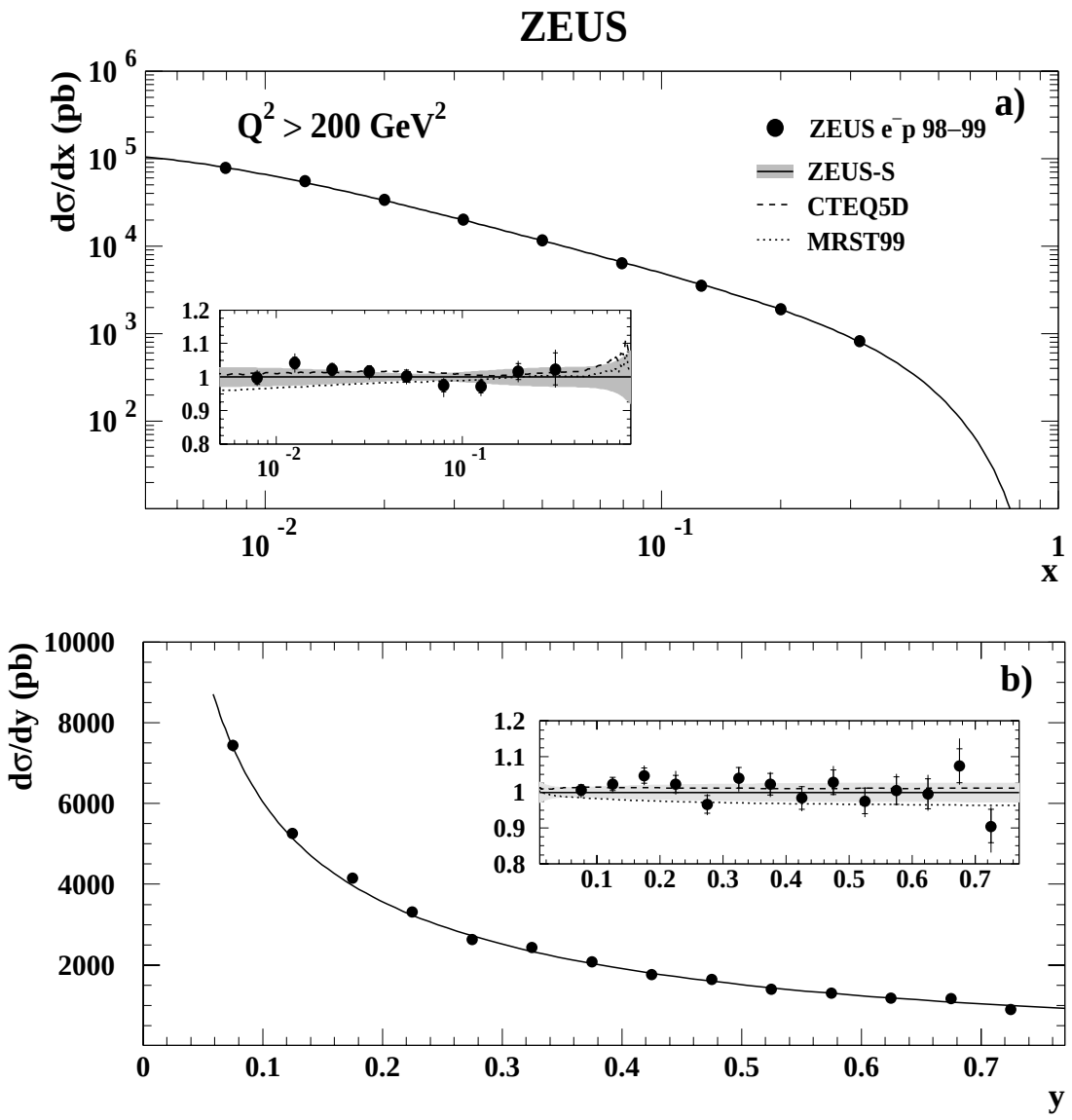

Figure 4: *a) The differential e^-p cross-section $d\sigma/dx$ for $Q^2 > 200\,GeV^2$ as a function of x compared to the SM expectation evaluated using the ZEUS-S fit. b) The differential e^-p cross-section $d\sigma/dy$ for $Q^2 > 200\,GeV^2$ as a function of y compared to the SM expectation evaluated using the ZEUS-S fit. The insets show ratios of the measured cross sections to the ZEUS-S predictions. Also shown are the ratios of SM prediction using CTEQ5D and MRST99 PDFs to that of ZEUS-S. The shaded band indicates the uncertainty on the calculated cross section due to the uncertainty in the ZEUS-S PDFs. The inner error bars of the measured points show the statistical uncertainty, while the outer ones show the statistical and systematic uncertainties added in quadrature.*

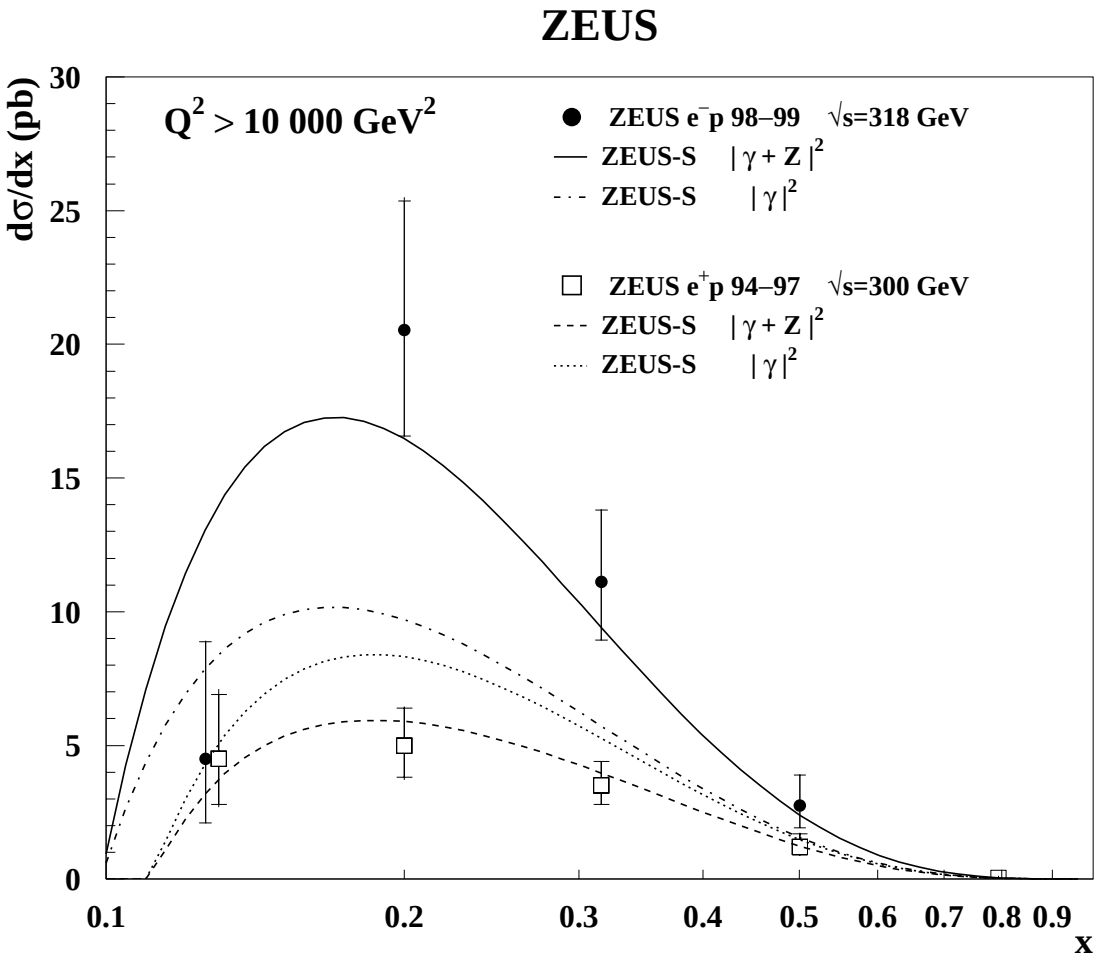

Figure 5: *Comparison of measured cross-sections $d\sigma/dx$ for e^-p (at $\sqrt{s} = 318\,GeV$) and e^+p (at $\sqrt{s} = 300\,GeV$) scattering as a function of x for $Q^2 > 10\,000\,GeV^2$. The cross sections calculated including the Z-exchange contribution are shown by the solid and dashed lines. The cross sections obtained from photon exchange only are shown by the dash-dotted and dotted lines. The lowest e^-p point in x is moved slightly to the left for clarity. The inner error bars show the statistical error, while the outer ones show the statistical and systematic uncertainties added in quadrature.*

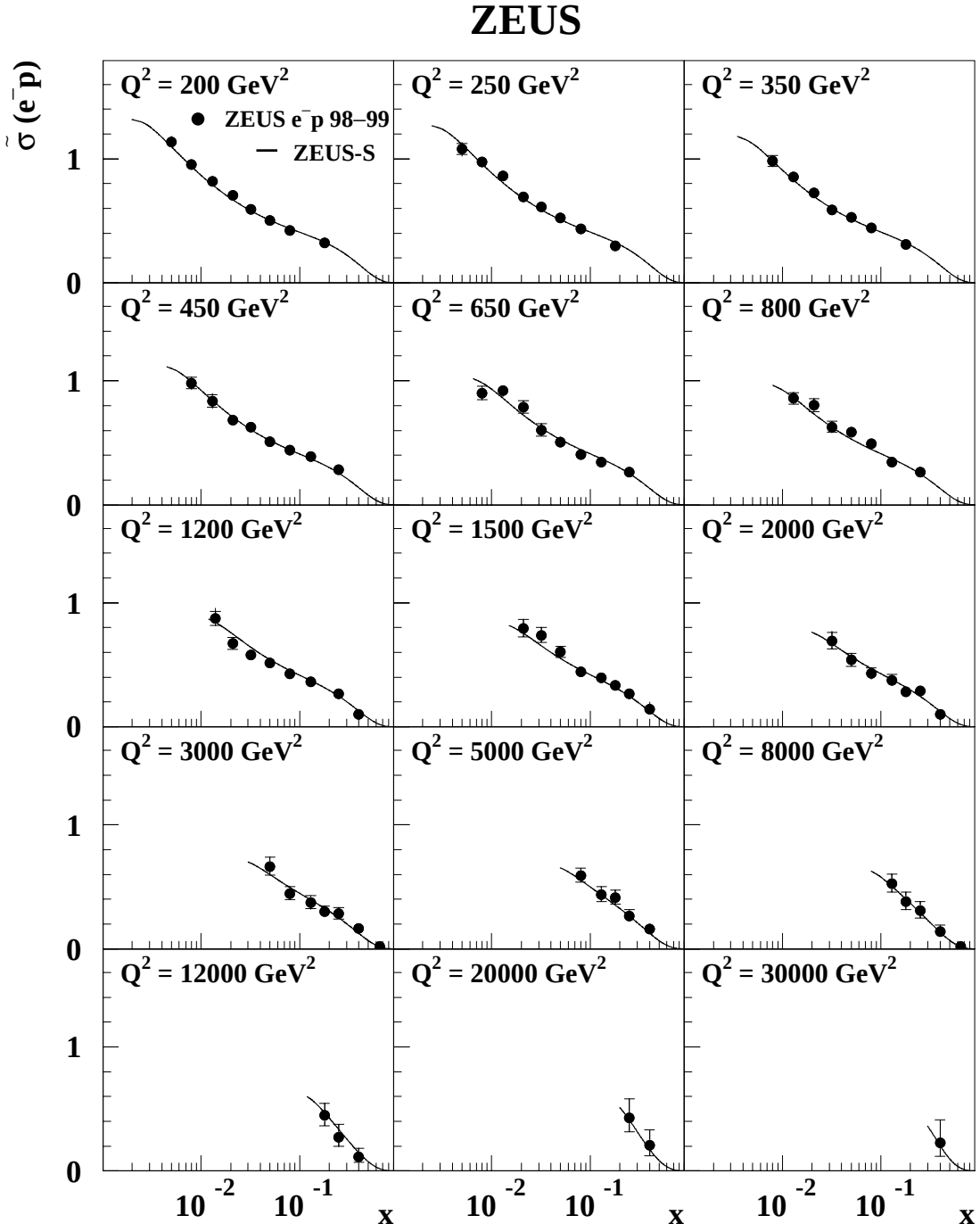

Figure 6: *The e^-p reduced cross-section $\tilde{\sigma}(e^-p)$ (solid points) plotted as a function of x at fixed Q^2 between 200 GeV^2 and 30 000 GeV^2. Also shown is the SM expectation evaluated using the ZEUS-S PDFs. The inner error bars show the statistical uncertainty, while the outer ones show the statistical and systematic uncertainties added in quadrature.*

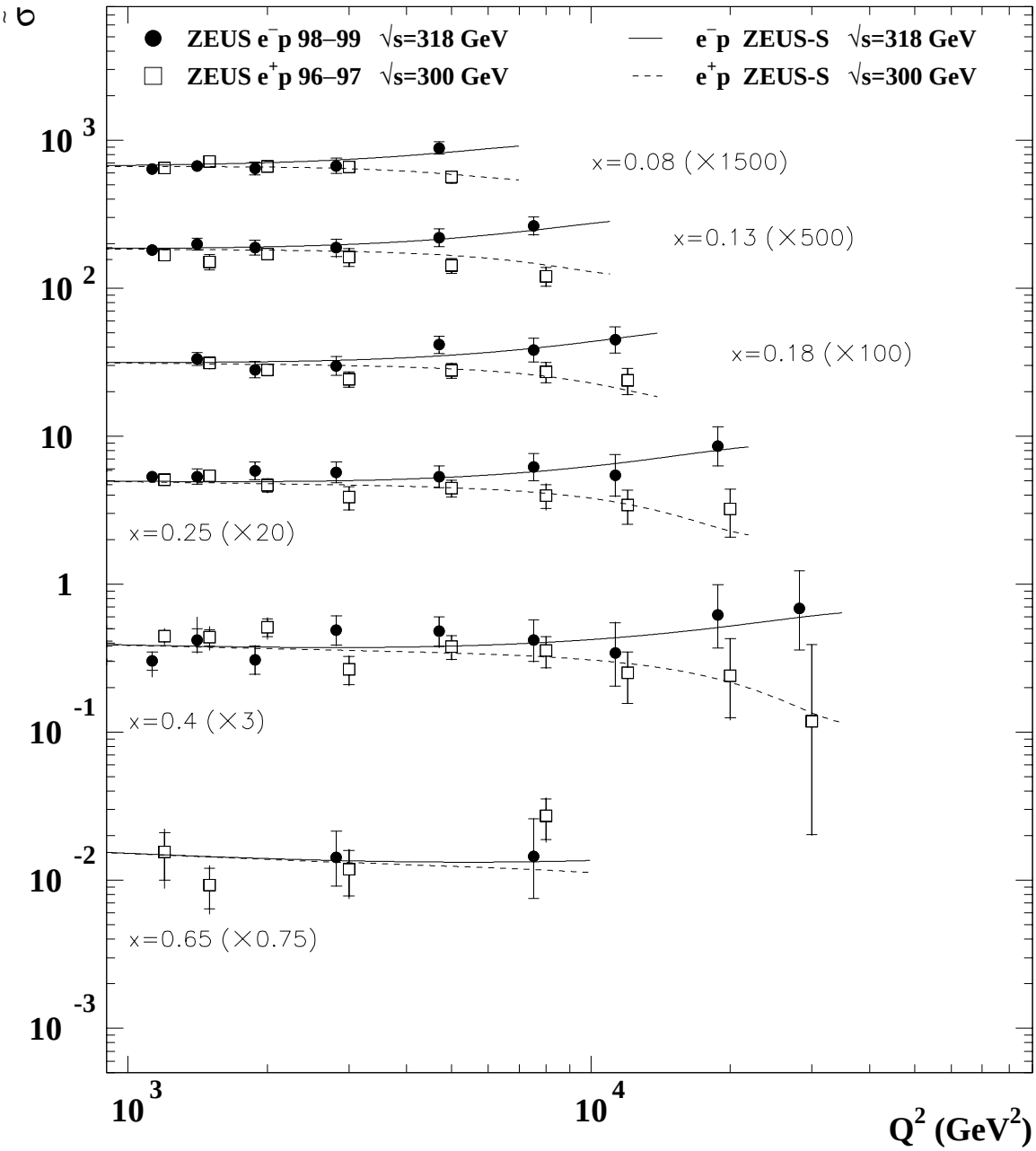

Figure 7: *The reduced cross-sections $\tilde{\sigma}$ for e^-p (solid points) and e^+p (open squares) scattering as a function of Q^2 in six different bins of x. All e^-p points are moved slightly to the left for clarity. The measured values are compared to theoretical predictions using the ZEUS-S PDFs. The inner error bars show the statistical uncertainty, while the outer ones show the statistical and systematic uncertainties added in quadrature. The reduced cross sections for a particular x value have been scaled by the number shown in parentheses.*

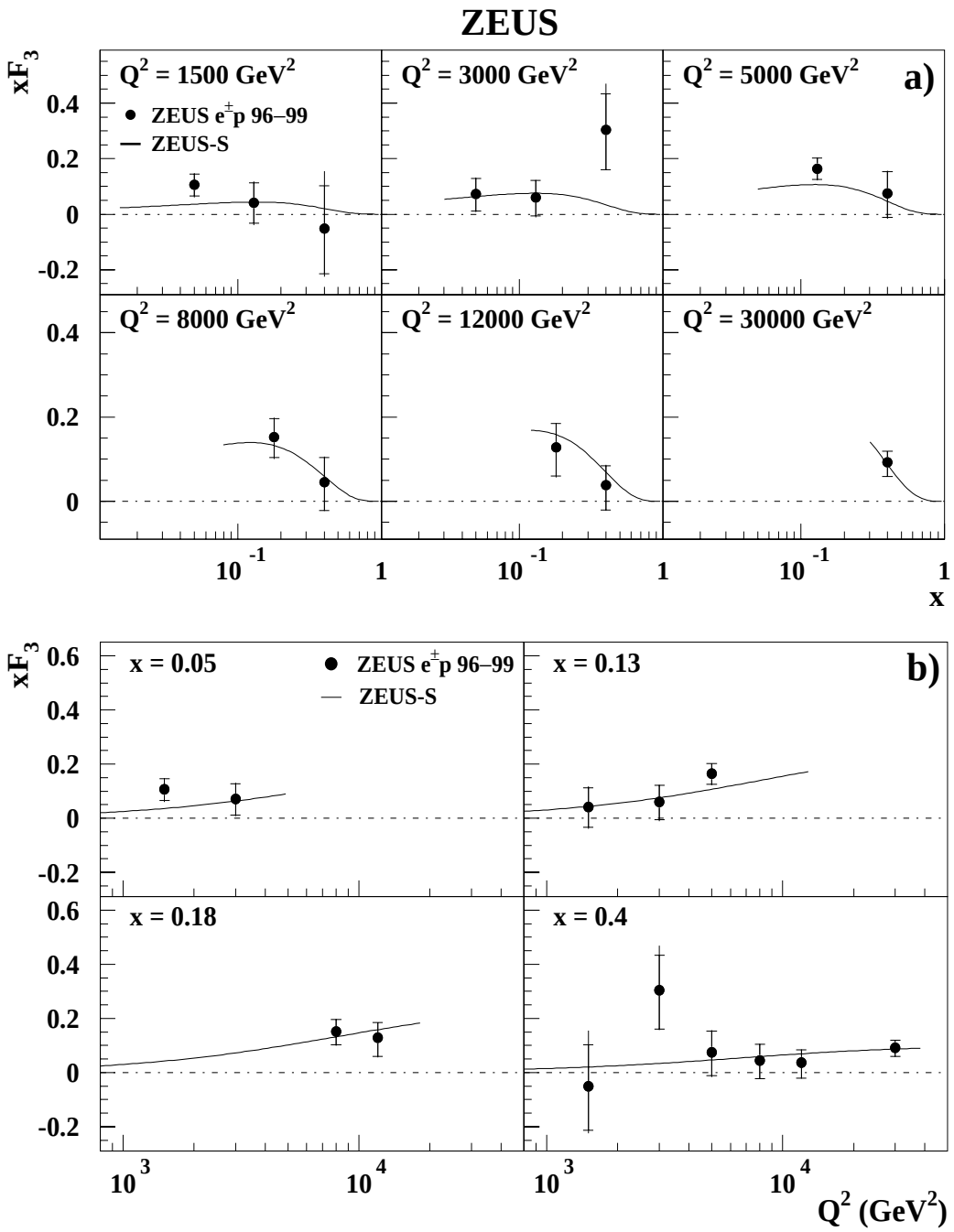

Figure 8: *The structure function xF_3 a) as a function of x for different Q^2 values and b) as a function of Q^2 for different x values. The inner error bars show the statistical uncertainty, while the outer ones show the statistical and systematic uncertainties added in quadrature. Also shown are SM calculations using the ZEUS-S PDFs.*

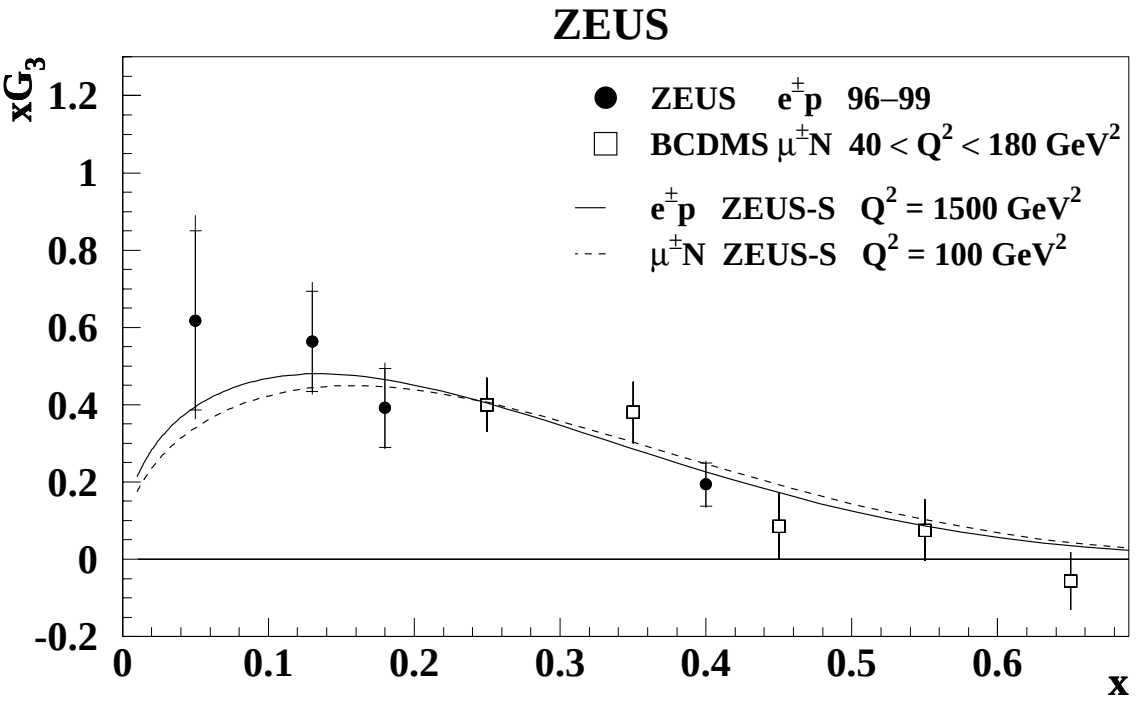

Figure 9: *The structure function xG_3 for $e^{\pm}p$ scattering (solid points) compared to that from BCDMS (open squares, total errors only). The prediction based on the ZEUS-S PDFs at $Q^2 = 1\,500\ GeV^2$ ($100\ GeV^2$) is shown as the solid (dashed) line.*